Cell Reports

The HAUS Complex Is a Key Regulator of Non-centrosomal Microtubule Organization during Neuronal Development

Graphical Abstract

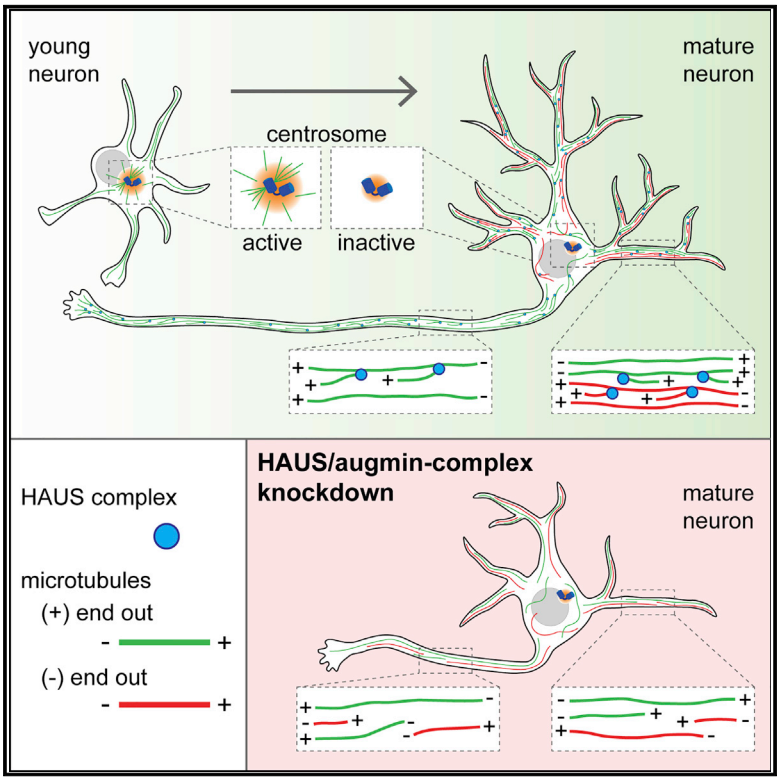

Highlights

- The HAUS/augmin complex regulates migration and polarization *in vivo*
- Axonal and dendritic development are regulated by HAUS/augmin complex
- HAUS/augmin regulates microtubule density in dendrites and polarity in axons
- Discrete clusters of HAUS/augmin regulate local microtubule nucleation in neurons

Authors

Inês Cunha-Ferreira, Anaël Chazeau, Robin R. Buijs, ..., R. Jeroen Pasterkamp, Lukas C. Kapitein, Casper C. Hoogenraad

Correspondence

l.kapitein@uu.nl (L.C.K.), c.hoogenraad@uu.nl (C.C.H.)

In Brief

Cunha-Ferreira et al. report that the HAUS/augmin complex regulates neuronal migration, polarization, and development. In neurons, the HAUS complex is distributed as discrete clusters regulating local microtubule nucleation. These findings shed light into how microtubules are generated in developing neurons after centrosome inactivation in early development.

Cunha-Ferreira et al., 2018, Cell Reports *24*, 791–800
July 24, 2018
https://doi.org/10.1016/j.celrep.2018.06.093

CellPress

Cell Reports
Report

The HAUS Complex Is a Key Regulator of Non-centrosomal Microtubule Organization during Neuronal Development

Inês Cunha-Ferreira,[1,4] Anaël Chazeau,[1,4] Robin R. Buijs,[1,4] Riccardo Stucchi,[1,2] Lena Will,[1] Xingxiu Pan,[1] Youri Adolfs,[3] Christiaan van der Meer,[3] Joanna C. Wolthuis,[1] Olga I. Kahn,[1] Philipp Schätzle,[1] Maarten Altelaar,[2] R. Jeroen Pasterkamp,[3] Lukas C. Kapitein,[1,*] and Casper C. Hoogenraad[1,5,*]

[1]Cell Biology, Department of Biology, Faculty of Science, Utrecht University, 3584 CH Utrecht, the Netherlands
[2]Biomolecular Mass Spectrometry and Proteomics, Bijvoet Center for Biomolecular Research and Utrecht Institute for Pharmaceutical Sciences, Utrecht University, 3584 CH Utrecht, the Netherlands
[3]Department of Translational Neuroscience, Brain Center Rudolf Magnus, University Medical Center Utrecht, Utrecht University, 3584 CG Utrecht, the Netherlands
[4]These authors contributed equally
[5]Lead Contact
*Correspondence: l.kapitein@uu.nl (L.C.K.), c.hoogenraad@uu.nl (C.C.H.)
https://doi.org/10.1016/j.celrep.2018.06.093

SUMMARY

Neuron morphology and function are highly dependent on proper organization of the cytoskeleton. In neurons, the centrosome is inactivated early in development, and acentrosomal microtubules are generated by mechanisms that are poorly understood. Here, we show that neuronal migration, development, and polarization depend on the multi-subunit protein HAUS/augmin complex, previously described to be required for mitotic spindle assembly in dividing cells. The HAUS complex is essential for neuronal microtubule organization by ensuring uniform microtubule polarity in axons and regulation of microtubule density in dendrites. Using live-cell imaging and high-resolution microscopy, we found that distinct HAUS clusters are distributed throughout neurons and colocalize with γ-TuRC, suggesting local microtubule nucleation events. We propose that the HAUS complex locally regulates microtubule nucleation events to control proper neuronal development.

INTRODUCTION

Microtubule (MT) assembly, organization, and remodeling are major determinants of neuronal morphology and function (Conde and Cáceres, 2009). In mammalian neurons, MTs are typically plus-end out in axons and of mixed polarity in dendrites, allowing directional transport of organelles and signaling molecules to specific compartments (Kapitein and Hoogenraad, 2015). Typically, MT nucleation is mediated by the centrosome and depends on γ-tubulin, which assembles into multi-subunit complexes, the γ-tubulin small complex (γ-TuSC) and the large γ-tubulin ring complex (γ-TuRC). Neurons, like other differentiated cells, undergo centrosome inactivation throughout development, and MT nucleation is reassigned at acentrosomal sites (Stiess et al., 2010; Sulimenko et al., 2017). Although great progress has been made regarding minus-end MT stabilization (Akhmanova and Hoogenraad, 2015), how acentrosomal MTs are generated in neurons is still an open question. Initial studies suggested that MTs originated from severing of pre-existing MTs nucleated from the centrosome (Baas et al., 2005). However, this mechanism fails to explain how MTs are generated in older neurons with inactive centrosomes. Dendritic MT nucleation has been suggested to occur at Golgi outposts in *Drosophila* (Ori-McKenney et al., 2012; Yalgin et al., 2015; Zhou et al., 2014). However, Golgi outposts are absent from dendrites that require MT nucleation for development (Nguyen et al., 2014).

MTs can be also generated on other MTs in a process that depends on the γ-TuRC complex (Goshima et al., 2008; Lawo et al., 2009; Petry et al., 2011). In mammals, this process depends on a complex of eight subunits termed the HAUS/augmin complex (Lawo et al., 2009; Uehara et al., 2009). Initially identified in *Drosophila* (Goshima et al., 2007), HAUS/augmin subunits have been found to regulate mitotic spindle assembly in *Drosophila* and human cells or cortical MT organization in plants (Goshima et al., 2008; Lawo et al., 2009; Liu et al., 2014). Real-time visualization of HAUS-dependent MT nucleation in *X. laevis* meiotic extracts (Petry et al., 2011, 2013) and *Arabidopsis* cortical epidermal pavement cells (Liu et al., 2014) unraveled a key feature of this complex: generation of MTs with conserved polarity (Kamasaki et al., 2013; Petry et al., 2013). Recently the HAUS complex was suggested to regulate uniform MT polarity and density in axons (Sánchez-Huertas et al., 2016). However, it remains unknown where the HAUS complex localizes in neurons, whether HAUS can nucleate MTs, and to what extent HAUS is required for development.

In this study, we assess the role of the HAUS complex during neuronal development and polarization. We show that HAUS is required for neuronal migration, axonal and dendritic development, and MT organization. Furthermore, we characterize HAUS localization as discrete clusters that seem to engage in MT nucleation events. We propose a model whereby clusters

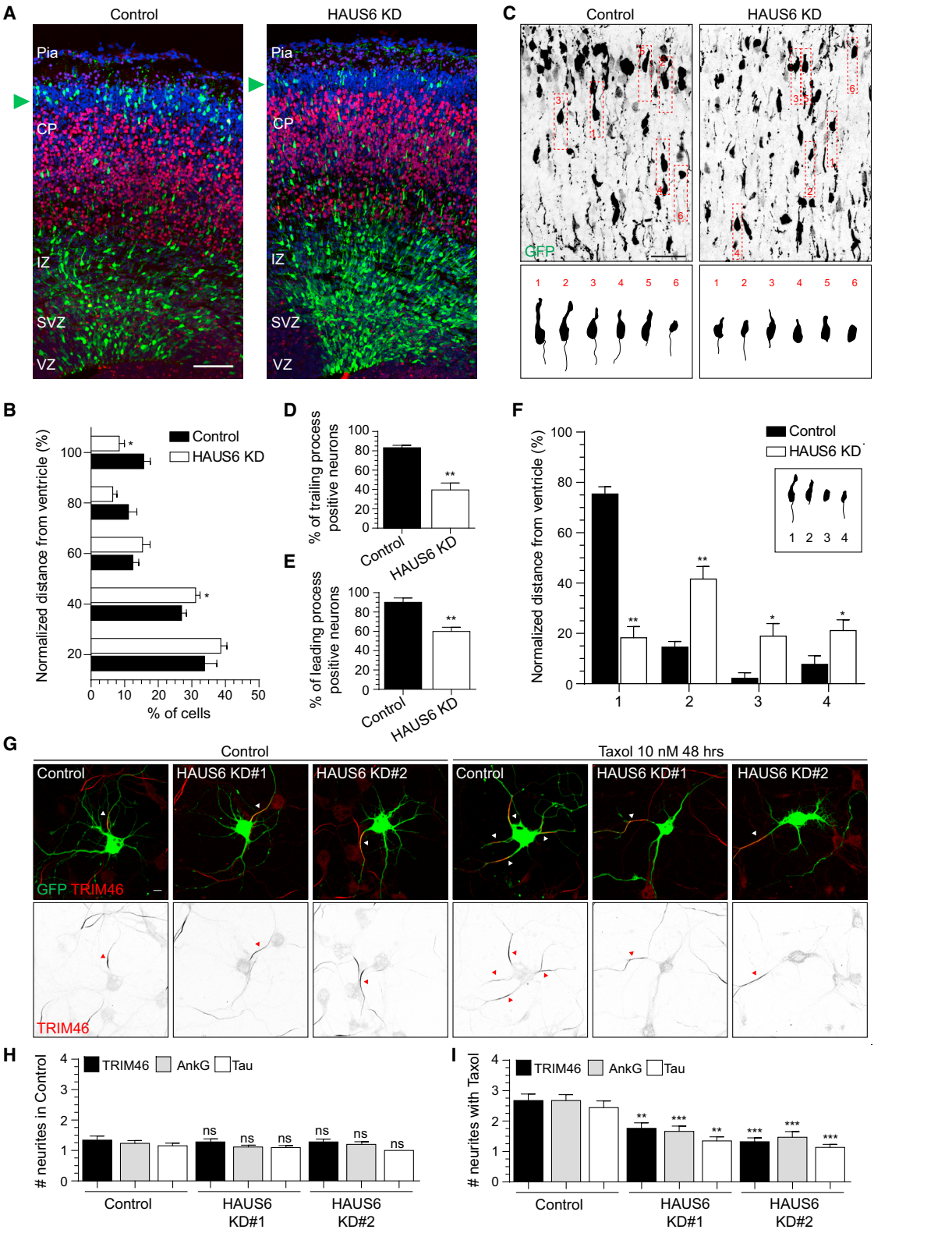

(legend on next page)

of the HAUS complex mediate MT nucleation in neurons to ensure proper development.

RESULTS

The HAUS Complex Is Required for Neuronal Migration, Axon Formation, and Polarization *In Vivo*

In the developing neocortex, neurons migrate from the ventricular zone across different layers toward the cortical plate (Barnes and Polleux, 2009). To test whether the HAUS complex is involved in neuronal migration, we performed *in utero* electroporation of E14.5 mouse embryos using short hairpin RNAs (shRNAs) targeting murine HAUS6 and a GFP plasmid to allow the identification of electroporated neurons (Figures 1A and 1B). We confirmed the efficiency of shRNA-mediated HAUS6 knockdown in murine IMCD3 cells, which showed impaired mitotic progression and increased spindle abnormalities (Figures S1A–S1C) as previously reported (Lawo et al., 2009). Following electroporation, embryos developed 3 additional days *in utero* before analysis. While control neurons reached the upper cortical layers, depletion of HAUS6 impaired migration and neurons remained in the sub-ventricular and intermediate zones (Figures 1A and 1B). During migration, neurons polarize and develop a trailing process that later becomes the axon and a leading edge that will develop as the apical dendrite. In our experiments, most GFP-positive control neurons showed bipolar morphology, whereas neurons depleted of HAUS6 lacked the trailing (~53% compared with control) and leading (~33% compared with control) (Figures 1C–1F) processes. Together these data show that the HAUS complex is required for axon formation, neuronal polarization, and migration *in vivo*.

The HAUS Complex Is Required for Axon Specification *In Vitro*

The first step in neuron polarization is axon formation. It is well known that increased MT stability along the neuritic shaft precedes axon formation and that MT dynamics drives polarization. Furthermore, the MT-stabilizing drug Taxol was shown to induce the formation of supernumerary axons (Witte et al., 2008). To test whether the HAUS complex is required for multiple axon formation, we combined Taxol treatment with HAUS6 depletion (Figures 1G–1I and S1D). We designed two separate shRNAs against HAUS6 and confirmed their efficiency by immunocytochemistry (Figures S1E–S1I). In control, Taxol treatment increased the mean number of processes positive for three axonal markers, TRIM46, AnkG, and Tau. By contrast, knockdown of HAUS6 prevented the formation of supernumerary axons in the presence of Taxol (Figures 1G–1I and S1D). These data show that HAUS is required for the formation of axons upon stabilization of MTs with Taxol *in vitro*. In addition, supernumerary axons positive for TRIM46, an early instructor in axon polarization (van Beuningen et al., 2015), fail to assemble after HAUS depletion, indicating that HAUS is required at an early stage of axon specification.

The HAUS Complex Regulates Axonal and Dendritic Development

To assess whether HAUS is required for axonal development, we designed additional shRNAs for HAUS2. Axonal arborization was analyzed at day *in vitro* (DIV) 5 after depletion of HAUS2, HAUS6, and the positive control γ-tubulin (Yau et al., 2014). HAUS2 and HAUS6 knockdown severely impaired axonal growth, similar to γ-tubulin depletion (Figures 2A and 2B). Contrary to HAUS depletion, overexpression of GFP-HAUS2 or GFP-HAUS6 had no effect on total axon arborization (Figures 2C, 2D, and S2A). Co-expression of GFP-HAUS2 and GFP-HAUS6 rescued their respective axonal phenotypes (Figures 2C, 2D, and S2A). We also determined the effect of HAUS2 and HAUS6 depletion on dendritic development using Sholl analysis. Depletion of HAUS2 and HAUS6 phenocopied γ-tubulin depletion with a reduction in total dendritic branching and complexity compared with controls (Figures 2E–2G and 2J). We were able to partially rescue knockdown phenotypes with GFP-HAUS2 and GFP-HAUS6 co-transfection, and overexpression of GFP-HAUS2 or GFP-HAUS6 alone did not alter dendritic complexity (Figures 2H, 2I, 2K, 2L, and S2B). Collectively, these data show that the HAUS complex is required for both axonal and dendritic development in hippocampal neurons.

The HAUS Complex Is Required for MT Organization in Axons and Dendrites

To test whether the HAUS complex is required for MT organization in neurons, we investigated the consequences of depleting HAUS6 on the cytoskeleton. The number of MT plus-ends (EB3) was analyzed along proximal dendrites after HAUS6 depletion at DIV12. In HAUS6-depleted neurons, the number of EB3 comets was reduced by ~48% (Figures 3A and 3B). This

Figure 1. The HAUS Complex Regulates Neuronal Migration and Polarization *In Vivo*

(A) Low magnification stitched maximum-intensity projection and quantification of migrating neurons in E17.5 mouse cortex positively electroporated *in utero* at E14.5 with GFP and pSuper control or HAUS6 shRNAs. CP, cortical plate; IZ, intermediate zone; Pia, Pial surface; SVZ, sub-ventricular zone; VZ, ventricular zone. Green, GFP; red, Ctip2; blue, DAPI. GFP-positive neurons at the pial surface are indicated with a green arrowhead.

(B) Normalized migration distribution along the radial axis from the ventricle to the pial surface of GFP-positive neurons (n = 15 or 16, N = 6).

(C) High-magnification maximum-intensity projections of E17.5 mouse cortical neurons positively electroporated *in utero* at E14.5 with GFP and pSuper control or HAUS6 shRNAs.

(D and E) Percentage of trailing (D) or leading process-positive (E) neurons in pSuper control and HAUS6 shRNAs electroporated brains (n = 51–92, N = 3).

(F) Quantification of neuronal morphology in pSuper control and HAUS6 shRNAs electroporated brains (n = 51–92, N = 3).

(G) DIV6 hippocampal neurons co-transfected with pSuper control, HAUS6 knockdown (KD) #1, 2 shRNAs and GFP at DIV2 and treated at DIV4 with control vehicle (DMSO) or Taxol. Green, GFP; red, TRIM46. TRIM46-positive processes are highlighted with a white arrowhead in merged images and red arrowhead in gray-scale inverted images.

(H and I) Average number of processes positive for TRIM46, AnkG, and Tau in control (H) and Taxol treatment (I) (n = 18–34, N = 3 for TRIM46 and AnkG; N = 2 for Tau).

Graphs represent the mean ± SEM. *p < 0.05, **p < 0.01, ***p < 0.001. Scale bars, 100 μm in (A), 40 μm in (C), and 10 μm in (G). See also Figure S1 and Table S1.

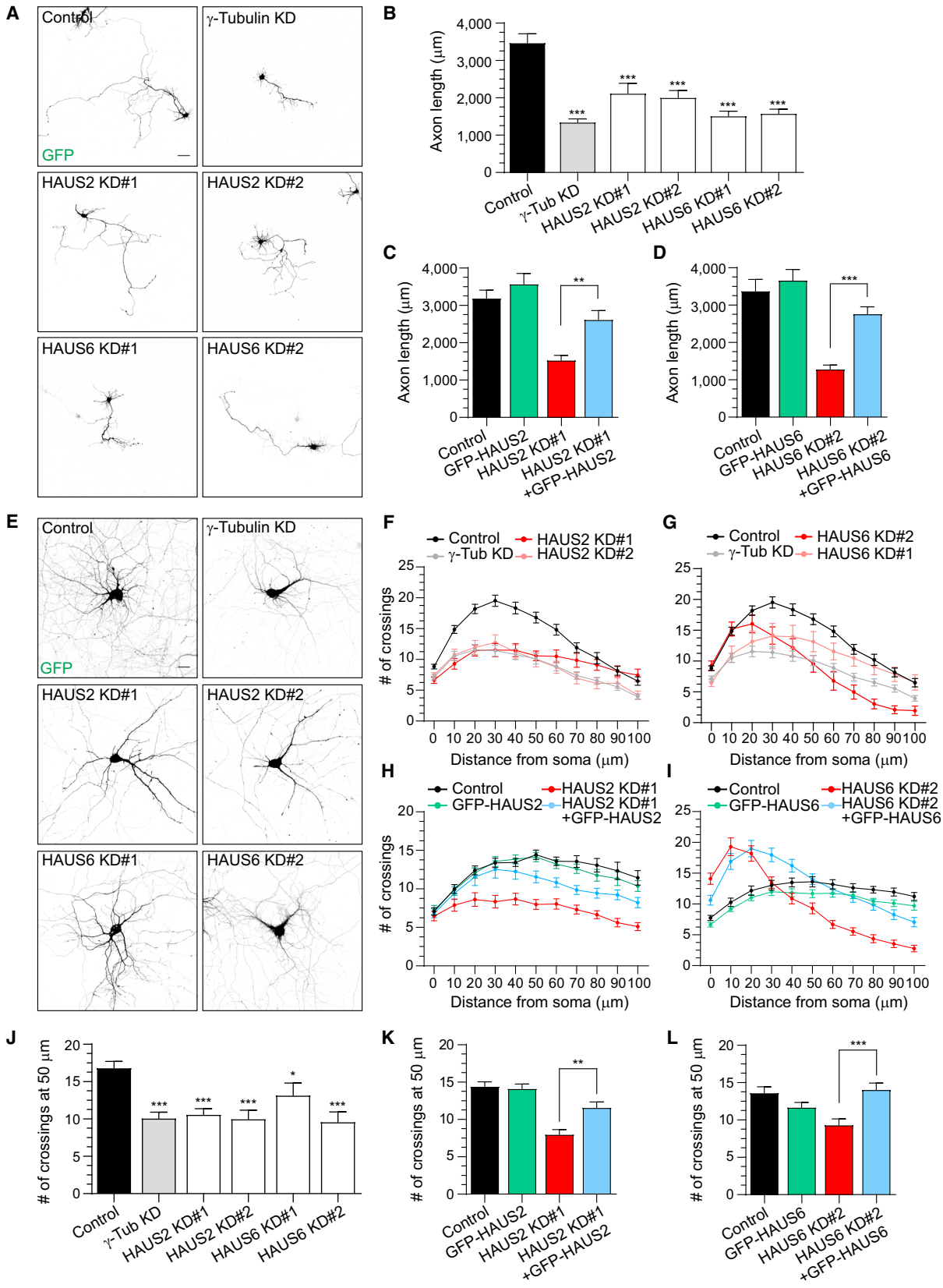

(legend on next page)

decrease was also found in the soma (data not shown). In line with these results, MAP2 (dendritic MT-associated protein) intensity was reduced by ~44% in proximal dendrites of HAUS6-depleted neurons (Figures 3A and 3C). To investigate if HAUS is required for maintenance of neuronal MTs, levels of polymerized tubulin were analyzed after a pre-extraction protocol that allows the extraction of soluble tubulin. Depletion of HAUS6 led to a ~31% reduction of polymerized α-tubulin in dendrites of DIV11 neurons (Figures 3D and 3E). Total levels of α-tubulin were not changed after depletion of HAUS6, indicating that this effect is specific for polymerized α-tubulin (Figures S2C and S2D). More specifically, tyrosinated tubulin (a marker of newly assembled MTs) and acetylated tubulin (a marker of stable MTs) levels showed reductions of ~13% and 23%, respectively, in HAUS6-depleted neurons (Figures 3F–3H). As for α-tubulin, western blot analysis showed no changes in the total pool of these proteins (Figures S2E–S2H). Taken together, these results reveal that HAUS is required for the maintenance of MT density in dendrites.

To test if HAUS regulates MT polarity in axons, we analyzed the orientation of MTs live using a GFP-MT+TIP marker in DIV11 neurons depleted of HAUS6. HAUS6 depletion increased the percentage of retrograde comets in axons ~2.5-fold, showing that HAUS regulates MT polarity in axons (Figures S2I–S2K; Video S1), as previously reported (Sánchez-Huertas et al., 2016). In mature dendrites, dynamic MTs are maintained at a ratio of 20% minus-end out and 80% plus-end out (Yau et al., 2016). In contrast to axons, HAUS6 depletion did not change MT polarity in dendrites (Figure S2L). Collectively, these data indicate that the HAUS complex regulates the MT cytoskeleton in neurons by maintaining MT polarity in axons and density in dendrites.

The HAUS Complex Colocalizes with the γ-TuRC in Discrete Clusters in Neurons

To gain insight into the function of the HAUS complex in neurons, we analyzed the localization of GFP-HAUS2. In young neurons (DIV2/4), GFP-HAUS2 localized to centrioles, as discrete clusters in the soma and along the axon (Figures S3A and S3B). GFP-HAUS2 and mCherry-HAUS6 co-expressed at DIV10–11 showed both proteins localizing at centrioles and in clusters present in soma and dendrites. HAUS2 and HAUS6 colocalized ~68% in clusters, suggesting that the majority of clusters represent complexes containing different HAUS subunits (Figures 4A, 4B, and S3C). Furthermore, depletion of HAUS6 reduced the number of GFP-HAUS2 clusters in DIV12–15 neurons (Figures 4C and 4D). This result is in line with the observation that HAUS complex subunit localization is interdependent (Lawo et al., 2009).

Analysis of GFP-HAUS2 cluster motility in proximal dendrites of DIV10–11 neurons showed that ~73% of clusters are immobile (Figures 4E–4G; Video S2). Remaining HAUS clusters mostly showed anterograde and retrograde mobility at ~50% ratio (Figures 4E–4J; Video S2). To gain further insight into the mechanism underlying HAUS localization and dynamics, we searched for putative binding partners of the HAUS complex. To this end, lysates of HEK293 cells co-expressing Bio-GFP-HAUS2 or HAUS6 and the biotin-protein ligase BirA were incubated with adult brain extracts, and isolated proteins were analyzed by affinity purification-mass spectrometry (AP-MS). All subunits of the HAUS complex were co-affinity-purified in HEK293 cells (Figure S4A) as previously reported (Lawo et al., 2009). Affinity purification of HAUS2 and HAUS6 brought down various α- and β-tubulin subunits and MT-associated proteins in rat adult brains (Figures S4B–S4E), consistent with the association of the HAUS complex with the MT cytoskeleton (Sánchez-Huertas and Lüders, 2015). Interestingly, several actin-related proteins were enriched in the list of proteins pulled down with HAUS6 (Figures S4B–S4D). Analysis of protein interaction networks (Cytoscape, GeneMANIA plugin) revealed how these proteins are interconnected (Figure S4B). To better map the localization of the HAUS complex with respect to actin and MTs, we performed three-color super-resolution imaging (see Supplemental Experimental Procedures for details). In DIV4 neurons, GFP-HAUS2 clusters colocalized with the MT cytoskeleton. Surprisingly, GFP-HAUS2 clusters also localized to the actin cytoskeleton (Figures S4F and S4G). Although most clusters colocalized with both actin and MTs, some GFP-HAUS2 clusters localized exclusively to actin. These data suggest that GFP-HAUS2 clusters may associate both with the MT and the actin cytoskeleton.

Interestingly, in plants, MT nucleation events are associated with discrete, immobile HAUS clusters along cortical MTs (Liu et al., 2014). To address whether HAUS clusters nucleate MTs in neurons we tested for colocalization with the γ-TuRC complex. GFP-HAUS2 and GCP2-mCherry showed ~45% colocalization, suggesting that approximately half of HAUS clusters are potential MT nucleation sites (Figures 4A, 4B, and S3C). Additionally, growing MT plus tips were found emerging from GFP-labeled HAUS2 clusters in several instances, suggesting that these represent authentic MT nucleation sites in neurons (Figures 4K, 4L, and S3D; Video S3). Collectively, these data suggest that the HAUS complex localizes as discrete clusters along the neuronal cell body and processes to allow local MT nucleation events.

Figure 2. The HAUS Complex Regulates Axonal and Dendritic Development *In Vitro*

(A) DIV5 hippocampal neurons co-transfected with GFP and pSuper control, HAUS2 KD#1, 2, HAUS6 KD#1, 2 or γ-tubulin shRNAs.

(B) Axon arborization related to (A) (n = 18–20, N = 2).

(C and D) Axon arborization of DIV5 neurons co-transfected with HA-β-galactosidase and pSuper control, HAUS2 KD#1 (C) or HAUS6 KD#2 (D) with GFP, GFP-HAUS2 or GFP HAUS6 shRNA resistant (n = 18–24 in C, n = 19–22 in D, N = 2).

(E) DIV12 hippocampal neurons co-transfected with GFP and pSuper control, HAUS2 KD#1, 2, HAUS6 KD#1, 2 or γ-tubulin shRNAs.

(F and G) Sholl analysis related to (E) (n = 20–46, N = 2; the control in F and G is the same because these are data from one common set of experiments).

(H and I) Sholl analysis of DIV12 hippocampal neurons co-transfected with HA-β-galactosidase and pSuper control, HAUS2 KD#1 (H) or HAUS6 KD#2 (I) with GFP, GFP-HAUS2 or GFP HAUS6 shRNA resistant (n = 20, N = 2 in H; n = 30, N = 3 in I).

(J) Average number of crossings at 50 μm distance from the cell body related to (F) and (G).

(K and L) Average number of crossings at 50 μm distance from the cell body related to (H) and (I).

Graphs represent the mean ± SEM. *p < 0.05, **p < 0.01, ***p < 0.001. Scale bars, 50 μm in (A) and 20 μm in (E). See also Figure S2 and Table S1.

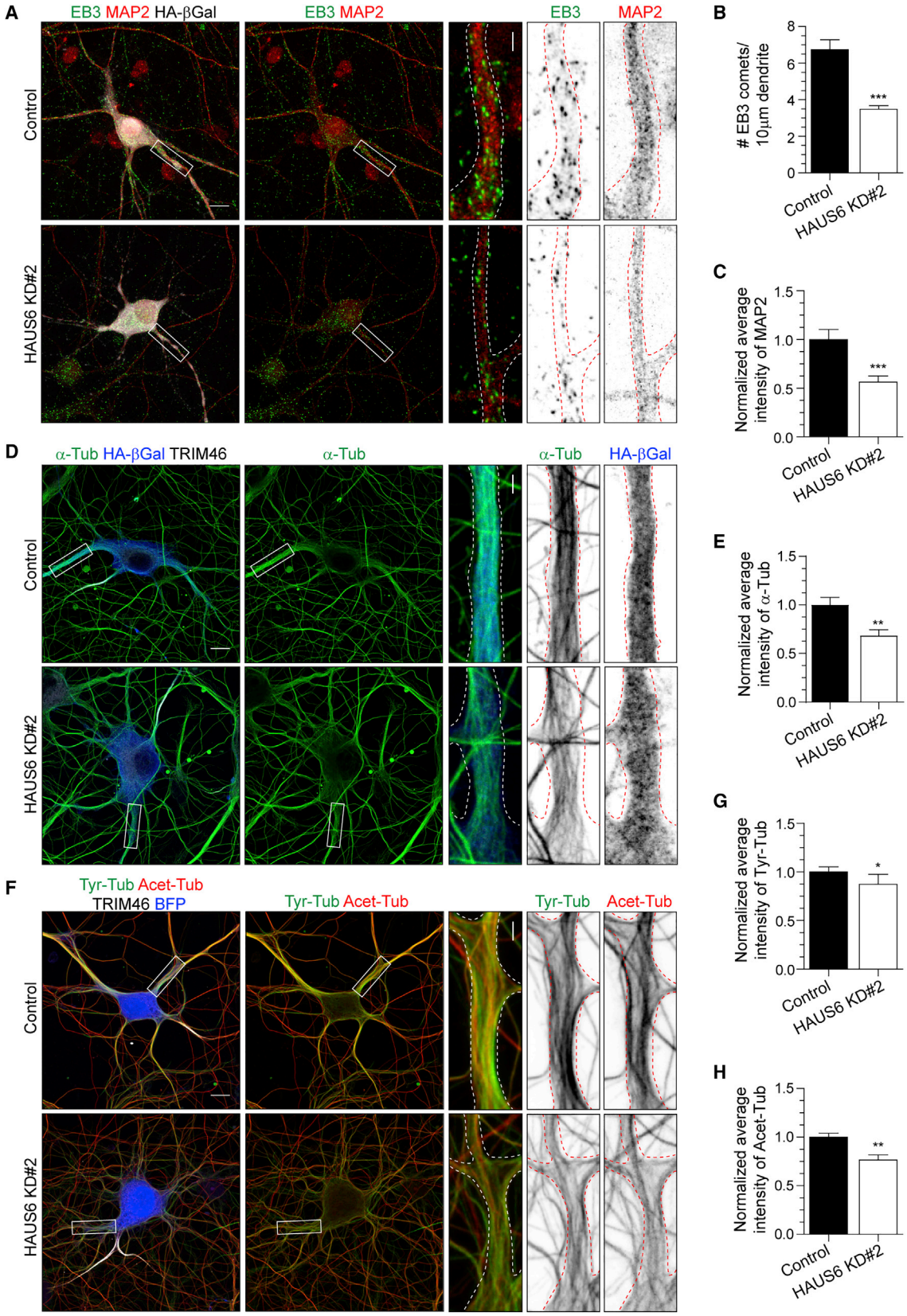

(legend on next page)

DISCUSSION

The ability of neurons to migrate, polarize, and differentiate depends on the MT cytoskeleton (Barnes and Polleux, 2009). In this paper, we demonstrate that the HAUS complex is required for neuronal migration, polarization, and development. Interestingly, some processes occur at a stage when the centrosome is actively nucleating MTs in neurons. These data suggest that both centrosomal and acentrosomal MT nucleation occurs at the same time during early development. One main feature of the HAUS complex is generation of MTs with conserved polarity (Kamasaki et al., 2013; Petry et al., 2013). Consistent with this, depletion of HAUS6 increased the percentage of retrograde growing MTs in axons, as previously reported by Sánchez-Huertas et al. (2016). Recent findings showing that HAUS additionally regulates MT density in axons (Sánchez-Huertas et al., 2016) suggest that HAUS mediates MT nucleation in axons to ensure MT polarity. Similarly to γ-tubulin, we found that the HAUS complex regulates neuronal polarity and axonal development, supporting the idea that HAUS-mediated MT nucleation regulates early neuronal development.

One stage of neuronal development that is likely to depend exclusively on acentrosomal MT nucleation is dendritic outgrowth, because at this stage the centrosome is fully inactivated (Nguyen et al., 2011, 2014; Ori-McKenney et al., 2012; Sánchez-Huertas et al., 2016; Stiess et al., 2010; Yau et al., 2014). In fact, γ-tubulin has been found to localize in dendrites and multiple MT growing ends emerge from varied sites suggesting that MTs are locally nucleated (Nguyen et al., 2014; Ori-McKenney et al., 2012; Yau et al., 2014). We found that depletion of the HAUS complex decreases MT density and impairs dendritic development. Depletion of HAUS6 led to a decrease in dynamic MTs (EB3), MAP2, α-tubulin, and tyrosinated tubulin. Contrary to a previous report by Sánchez-Huertas et al. (2016), we found that acetylated tubulin levels are also reduced in hippocampal neurons after depletion of HAUS6. This most likely reflects differences in analysis: Sánchez-Huertas et al. (2016) investigated axons of young neurons (DIV4), whereas our analysis was performed in dendrites of older neurons (DIV11–12). Axons are highly enriched in acetylated tubulin, so one may perhaps expect that depletion of HAUS in young neurons would not impair total levels of acetylated tubulin. Contrary to axons, HAUS6 depletion had no impact on MT polarity in dendrites, suggesting that antiparallel MT organization is regulated by alternative mechanisms (Kapitein and Hoogenraad, 2015). We propose that HAUS acts on dendritic MTs with already established polarity and regulates MT density within MT bundles (Tas et al., 2017). Collectively, these data suggest that the function of the HAUS complex is broader than previously anticipated. It is critical for neuronal migration, polarization, and development through local regulation of the MT cytoskeleton in axons and dendrites.

As in other systems (Lawo et al., 2009), localization of different HAUS subunits is interdependent in neurons, indicating that HAUS clusters represent sites of assembly for HAUS subunits into one complex. Furthermore, our findings that GCP2, a member of the γ-TuRC, colocalizes with HAUS and that dynamic MTs emerge from HAUS clusters strongly suggests that HAUS mediates local MT nucleation. We also observed a small population of HAUS2 clusters that did not colocalize with HAUS6 and GCP2. Those clusters likely represent immature complexes that are still undergoing assembly. Similar mechanisms are used in interphase pavement cells in *Arabidopsis* (Liu et al., 2014). A key signature of the HAUS complex is the generation of MTs along mother MTs: branched MT nucleation (Sánchez-Huertas and Lüders, 2015). Here we found that GFP-HAUS2 clusters colocalize with MTs, which could indicate that branched MT nucleation occurs in neurons. The high density of the MT cytoskeleton and/or the short lifespan of these MT configurations could explain why we have not been able to detect branched MTs in neurons. In fact, HAUS-nucleated MTs have been shown to be highly mobile or hardly detectable in other systems (Kamasaki et al., 2013; Lecland and Lüders, 2014; Liu et al., 2014; Petry et al., 2013).

Results from AP-MS indicate that the HAUS complex interacts with the actin and MT cytoskeleton in adult brains, suggesting that both cytoskeleton networks may cooperate with the HAUS complex to control local MT nucleation events. It is possible that MTs and actin contribute to the transport of HAUS subunits for complex assembly and local MT nucleation. In fact, ~27% of GFP-HAUS2 clusters are mobile. Unraveling the mechanism by which the actin or MT cytoskeleton regulates HAUS complex function is an interesting challenge for future studies.

In summary, we show that the HAUS complex regulates MT organization in neurons, playing an important role in neuronal polarization, development, and migration. HAUS appears as discrete clusters throughout the soma and neurites of hippocampal neurons, suggesting local MT nucleation. This work provides a novel mechanism whereby decentralized MT nucleation at HAUS clusters ensures proper MT remodeling during neuronal development.

Figure 3. The HAUS Complex Regulates MT Organization in Hippocampal Neurons

(A) DIV12 hippocampal neurons co-transfected with HA-β-galactosidase and pSuper control or HAUS6 KD#2 shRNAs. Insets depict dendrite areas. Green, EB3; red, MAP2; and gray, HA-β-galactosidase.

(B) Average number of EB3 comets per 10 μm proximal dendrite in DIV12 neurons related to (A) (n = 20, N = 2).

(C) Normalized average intensity of MAP2 at 10 μm proximal dendrite in DIV12 neurons related to (A) (n = 20, N = 2).

(D) DIV11 hippocampal neurons co-transfected with HA-β-galactosidase and pSuper control or HAUS6 KD#2 shRNAs. Insets depict dendrite areas. Green, α-tubulin; gray, TRIM46; and blue, HA-β-galactosidase.

(E) Normalized average intensity of α-tubulin at 10 μm proximal dendrite in DIV11 neurons related to (D) (n = 17, N = 2).

(F) DIV12 hippocampal neurons co-transfected with BFP and pSuper control or HAUS6 KD#2 shRNAs. Insets depict dendrite areas. Green, tyrosinated tubulin; red, acetylated tubulin; gray, TRIM46; blue, BFP.

(G and H) Normalized average intensity of tyrosinated (G) and acetylated (H) tubulin at 10 μm proximal dendrites of DIV11–12 neurons related to (F) (n = 17–19, N = 2).

Graphs represent the mean ± SEM. *p < 0.05, **p < 0.01, ***p < 0.001. Scale bars, 10 μm in panels and 2 μm in insets in (A), (D), and (F). See also Figure S2 and Table S1.

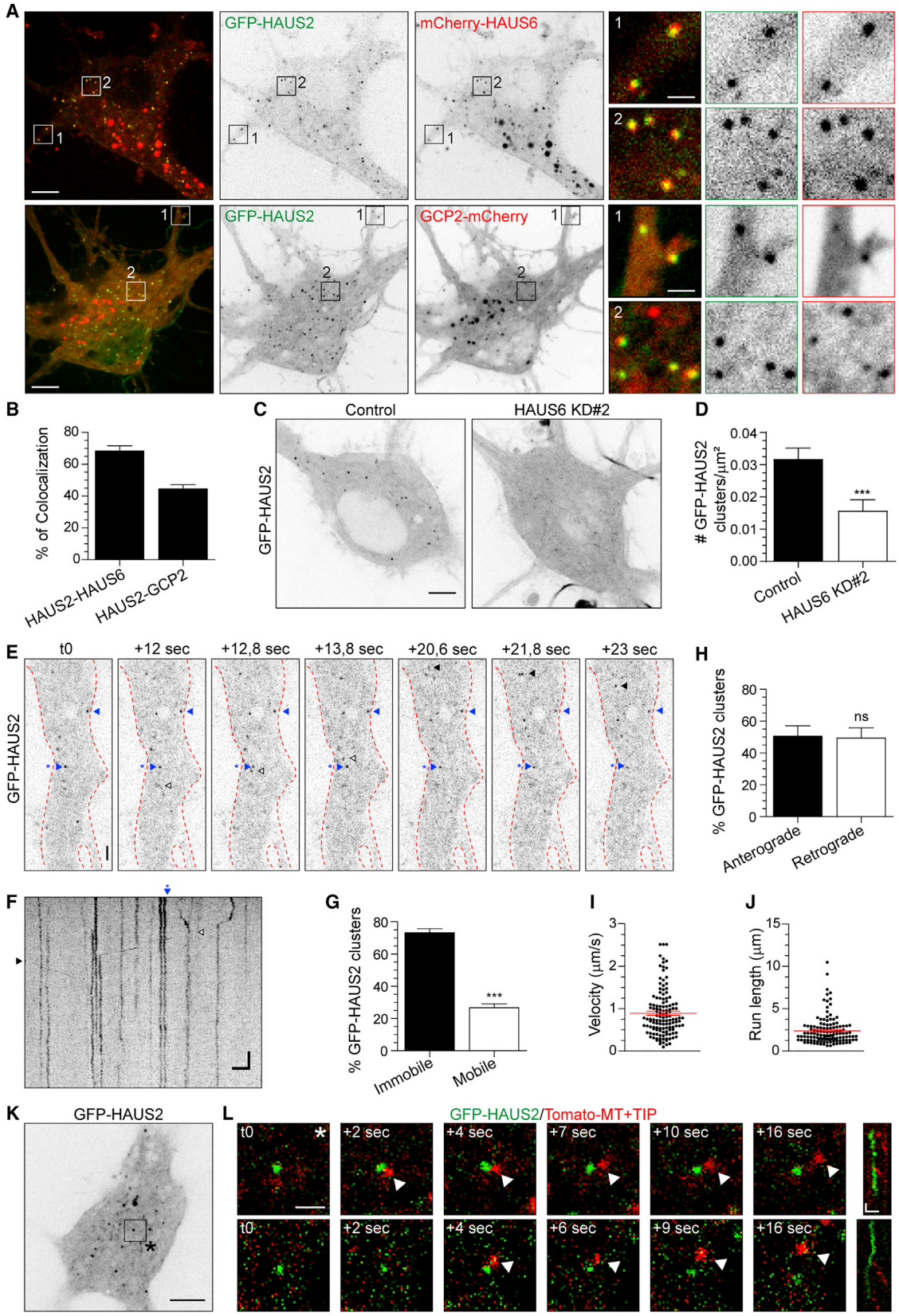

(legend on next page)

EXPERIMENTAL PROCEDURES

Further information and requests for resources and reagents should be directed to and will be fulfilled by the lead contact, Casper Hoogenraad (c.hoogenraad@uu.nl).

Animals

All experiments were approved by the Dutch Animal Experiments Committee (Dier Experimenten Commissie [DEC]), performed in line with institutional guidelines of University Utrecht and UMC (University Medical Center) Utrecht, and conducted in agreement with Dutch law (Wet op de Dierproeven, 1996) and European regulations (Directive 2010/63/EU). Female pregnant C57BL/6J mice were obtained from The Jackson Laboratory and female pregnant Wistar rats from Janvier. For *in utero* electroporation experiments, embryos of both genders were used at E14.5 stage of development. For hippocampal and cortical neuron culture experiments obtained from rat embryos, embryos of both genders at E18 stage of development were used. For further details see Supplemental Experimental Procedures.

Cell Lines

HEK293 cells (CRL1573) and mouse inner medullary collecting duct 3 (IMCD3) cells (CRL2123) were purchased from American Type Culture Collection (ATCC). Cell lines were not authenticated by the authors after purchase. For details on culturing conditions see Supplemental Experimental Procedures.

DNA and shRNA Constructs

pGW2-GFP-HAUS2 and HAUS6 were generated using a PCR-based strategy using pEGFP-C1-HAUS2 and pEGFP-C1-HAUS6 (a kind gift from Dr. Laurence Pelletier, Lunenfeld-Tanenbaum Research Institute). These constructs were used to reclone HAUS2/6 in pGW2-mCherry or Bio-GFP constructs. GCP2 was cloned in pGW2-mCherry by recloning it from pGW1-GCP2-GFP construct (a kind gift from Dr. Kah W. Yau and Dr. Kai Jiang, Department of Cell Biology, University of Utrecht). For further details on these and other constructs see Supplemental Experimental Procedures.

Antibodies and Reagents

The following antibodies were used in this study: rabbit anti-HAUS6 (Uehara et al., 2009), mouse anti-centrin clone 20H5 (04-1624; Millipore), rabbit anti-EB3 (02-1005-07; Stepanova et al., 2003), mouse anti-α-tubulin (T5168; Sigma-Aldrich), rat anti-tubulin tyrosinated clone YL1/2 (ab6160; Abcam), mouse anti-acetylated tubulin (T7451; Sigma-Aldrich). For more details on antibodies and reagents see Supplemental Experimental Procedures.

Primary Neuronal Cultures, Transfection, and Electroporation

Primary hippocampal and cortical cultures were prepared from embryonic day 18 (E18) rat brains (both genders). Hippocampal neurons were transfected with Lipofectamine 2000. Primary cortical neurons were electroporated using the Amaxa Rat Neuron Nucleofector kit (Lonza). For details see Supplemental Experimental Procedures.

In Utero Electroporation

In utero electroporation was performed as described previously (van Beuningen et al., 2015). For details see Supplemental Experimental Procedures.

AP-MS

Streptavidin beads pull-down assays were performed with HEK293 cells transfected with BirA and Bio-GFP-HAUS2, Bio-GFP-HAUS6, and Bio-GFP using polyethylenimine (PEI; Polysciences) for 48 hr according to the manufacturer's instructions. For further details see Supplemental Experimental Procedures.

Live Imaging and Super-resolution Imaging

Live imaging of neurons was performed using spinning-disk confocal microscopy with an inverted microscope Nikon Eclipse Ti-E or a Nikon Eclipse TE2000E. Three-color single molecule localization microscopy (SMLM) was performed on a Nikon Ti microscope. For further details see Supplemental Experimental Procedures.

Statistical Analysis

All data processing and statistical analysis were performed in Excel (Microsoft) and GraphPad Prism (GraphPad Software). Diagrams were made using GraphPad Prism. Significance was defined as follows: ns, not significant; $*p < 0.05$; $**p < 0.01$; and $***p < 0.001$. Statistical analyses included two-tailed unpaired t tests, Mann-Whitney U tests, Kruskal-Wallis tests followed by Dunn's multiple-comparison tests, one-way ANOVA followed by Holm-Sidak multiple-comparisons tests, Dunnett's multiple-comparisons tests, Sidak's multiple-comparisons tests or Tukey's multiple-comparisons tests, two-way ANOVA followed by Dunnett's multiple-comparisons tests or Tukey's multiple-comparisons tests, two-tailed chi-square tests with Yates's correction, and two-tailed Fisher's exact tests. The assumption of normality was tested using the D'Agostino-Pearson omnibus test. The exact values of n (total number of cells analyzed), N (total number of experiments), and statistical tests for each graph presented in the paper can be found in Table S1. N and n can also be found in figure legends.

SUPPLEMENTAL INFORMATION

Supplemental Information includes Supplemental Experimental Procedures, four figures, one table, and three videos and can be found with this article online at https://doi.org/10.1016/j.celrep.2018.06.093.

ACKNOWLEDGMENTS

We thank Gabriela Plucinska (Utrecht University) for critical reading of the manuscript. We thank Dr. Laurence Pelletier (Lunenfeld-Tanenbaum Research Institute) for sharing HAUS reagents and Dr. Ryota Uehara (Hokkaido University) and Prof. Gohta Goshima (Nagoya University) for the HAUS6 antibody. This work was supported by the following grants: Human Frontier Science Program fellowship LT000506/2013-L to I.C.-F.; the Netherlands Organization for Scientific Research (NWO), as part of the Graduate Programme project, grant

Figure 4. The HAUS Complex Colocalizes with the γ-Tubulin Complex at Acentrosomal Clusters in Hippocampal Neurons

(A) Average intensity projections of stream acquisitions of DIV10 hippocampal neurons expressing GFP-HAUS2 (green) and mCherry-HAUS6 (top) or GCP2-mCherry (bottom) (red). Insets depict indicated areas.

(B) Percentage of GFP-HAUS2 clusters colocalizing with mCherry-HAUS6 or GCP2-mCherry in DIV10–11 neurons (n = 28–51, N = 4).

(C) Average intensity projection of stream acquisition of DIV12 hippocampal neurons co-transfected with GFP-HAUS2 and pSuper control or HAUS6 KD#2 shRNAs.

(D) Density of GFP-HAUS2 clusters in DIV12–15 neurons (n = 43, N = 2).

(E and F) Stills (E) and kymograph (F) of GFP-HAUS2 in a proximal dendrite of a DIV10 neuron from 1 min stream acquisition. Time is in seconds. Anterograde and retrograde GFP-HAUS2 events are indicated with black and white arrowheads, respectively, and stationary events with blue arrowhead.

(G) Percentage of mobile and immobile GFP-HAUS2 clusters in DIV10–11 neurons (n = 24, N = 3).

(H) Percentage of anterograde and retrograde GFP-HAUS2 clusters in DIV10–11 neurons (n = 22, N = 3).

(I and J) Average velocity and run length of GFP-HAUS2 clusters in DIV10–11 neurons (n = 22, N = 3).

(K and L) Average intensity projection, stills (K) and kymographs (L) of 10 min time-lapse acquisitions of DIV17 neurons co-transfected with GFP-HAUS2 (green) and Tomato-MT+TIP (red). Top insets in (L) depict the area indicated in (K); bottom insets are from another neuron.

Graphs represent mean ± SEM. $***p < 0.001$. Scale bar, 5 μm in panels and 1 μm in insets in (A), 5 μm in (C), 2 μm in (E) and (F), 5 s in (F), 5 μm in (K), 1 μm in stills in (L), and 1 μm and 10 s in kymographs in (L). See also Figures S3 and S4 and Table S1.

022.003.003 to R.R.B.; European Research Council (ERC) Consolidator Grant 617050 to C.C.H.; ERC Starting Grant 336291 to L.C.K.; Marie Curie fellowship 661401 to A.C.; NWO grant NWO-ALW-VICI 865.10.010 to C.C.H.; grant NWO-ALW-VICI 865.14.004 to R.J.P.; grant NWO-ALW-VIDI 864.12.008 to L.C.K.; NWO, as part of the National Roadmap Large-Scale Research Facilities of the Netherlands, Proteins@Work, grant 184.032.201 to M.A.; and VIDI grant 723.012.102 to M.A.

AUTHOR CONTRIBUTIONS

Conceptualization, I.C.-F., C.C.H., and L.C.K.; Validation, I.C.-F., A.C., and R.R.B.; Formal Analysis, I.C.-F., A.C., R.R.B., R.S., X.P., and J.C.W.; Investigation, I.C.-F., A.C., R.R.B., R.S., L.W., X.P., Y.A., C.M., J.C.W., and O.I.K.; Resources, I.C.-F., R.R.B., J.C.W., P.S., C.C.H., R.J.P., and M.A.; Writing – Original Draft, I.C.-F. and C.C.H.; Writing – Review & Editing, I.C.-F. and C.C.H.; Visualization, I.C.-F., A.C., and R.R.B.; Supervision, C.C.H., L.C.K., R.J.P., and M.A.; Project Administration, C.C.H. and L.C.K.; Funding Acquisition, C.C.H., L.C.K., R.J.P., M.A., I.C.-F., A.C., and R.R.B.

DECLARATION OF INTERESTS

The authors declare no competing interests.

Received: November 10, 2017
Revised: April 13, 2018
Accepted: June 21, 2018
Published: July 24, 2018

REFERENCES

Akhmanova, A., and Hoogenraad, C.C. (2015). Microtubule minus-end-targeting proteins. Curr. Biol. *25*, R162–R171.

Baas, P.W., Karabay, A., and Qiang, L. (2005). Microtubules cut and run. Trends Cell Biol. *15*, 518–524.

Barnes, A.P., and Polleux, F. (2009). Establishment of axon-dendrite polarity in developing neurons. Annu. Rev. Neurosci. *32*, 347–381.

Conde, C., and Cáceres, A. (2009). Microtubule assembly, organization and dynamics in axons and dendrites. Nat. Rev. Neurosci. *10*, 319–332.

Goshima, G., Wollman, R., Goodwin, S.S., Zhang, N., Scholey, J.M., Vale, R.D., and Stuurman, N. (2007). Genes required for mitotic spindle assembly in Drosophila S2 cells. Science *316*, 417–421.

Goshima, G., Mayer, M., Zhang, N., Stuurman, N., and Vale, R.D. (2008). Augmin: a protein complex required for centrosome-independent microtubule generation within the spindle. J. Cell Biol. *181*, 421–429.

Kamasaki, T., O'Toole, E., Kita, S., Osumi, M., Usukura, J., McIntosh, J.R., and Goshima, G. (2013). Augmin-dependent microtubule nucleation at microtubule walls in the spindle. J. Cell Biol. *202*, 25–33.

Kapitein, L.C., and Hoogenraad, C.C. (2015). Building the neuronal microtubule cytoskeleton. Neuron *87*, 492–506.

Lawo, S., Bashkurov, M., Mullin, M., Ferreria, M.G., Kittler, R., Habermann, B., Tagliaferro, A., Poser, I., Hutchins, J.R., Hegemann, B., et al. (2009). HAUS, the 8-subunit human augmin complex, regulates centrosome and spindle integrity. Curr. Biol. *19*, 816–826.

Lecland, N., and Lüders, J. (2014). The dynamics of microtubule minus ends in the human mitotic spindle. Nat. Cell Biol. *16*, 770–778.

Liu, T., Tian, J., Wang, G., Yu, Y., Wang, C., Ma, Y., Zhang, X., Xia, G., Liu, B., and Kong, Z. (2014). Augmin triggers microtubule-dependent microtubule nucleation in interphase plant cells. Curr. Biol. *24*, 2708–2713.

Nguyen, M.M., Stone, M.C., and Rolls, M.M. (2011). Microtubules are organized independently of the centrosome in Drosophila neurons. Neural Dev. *6*, 38.

Nguyen, M.M., McCracken, C.J., Milner, E.S., Goetschius, D.J., Weiner, A.T., Long, M.K., Michael, N.L., Munro, S., and Rolls, M.M. (2014). γ-tubulin controls neuronal microtubule polarity independently of Golgi outposts. Mol. Biol. Cell *25*, 2039–2050.

Ori-McKenney, K.M., Jan, L.Y., and Jan, Y.N. (2012). Golgi outposts shape dendrite morphology by functioning as sites of acentrosomal microtubule nucleation in neurons. Neuron *76*, 921–930.

Petry, S., Pugieux, C., Nédélec, F.J., and Vale, R.D. (2011). Augmin promotes meiotic spindle formation and bipolarity in Xenopus egg extracts. Proc. Natl. Acad. Sci. U S A *108*, 14473–14478.

Petry, S., Groen, A.C., Ishihara, K., Mitchison, T.J., and Vale, R.D. (2013). Branching microtubule nucleation in Xenopus egg extracts mediated by augmin and TPX2. Cell *152*, 768–777.

Sánchez-Huertas, C., and Lüders, J. (2015). The augmin connection in the geometry of microtubule networks. Curr. Biol. *25*, R294–R299.

Sánchez-Huertas, C., Freixo, F., Viais, R., Lacasa, C., Soriano, E., and Lüders, J. (2016). Non-centrosomal nucleation mediated by augmin organizes microtubules in post-mitotic neurons and controls axonal microtubule polarity. Nat. Commun. *7*, 12187.

Stepanova, T., Slemmer, J., Hoogenraad, C.C., Lansbergen, G., Dortland, B., De Zeeuw, C.I., Grosveld, F., van Cappellen, G., Akhmanova, A., and Galjart, N. (2003). Visualization of microtubule growth in cultured neurons via the use of EB3-GFP (end-binding protein 3-green fluorescent protein). J. Neurosci. *23*, 2655–2664.

Stiess, M., Maghelli, N., Kapitein, L.C., Gomis-Rüth, S., Wilsch-Bräuninger, M., Hoogenraad, C.C., Tolić-Nørrelykke, I.M., and Bradke, F. (2010). Axon extension occurs independently of centrosomal microtubule nucleation. Science *327*, 704–707.

Sulimenko, V., Hájková, Z., Klebanovych, A., and Dráber, P. (2017). Regulation of microtubule nucleation mediated by γ-tubulin complexes. Protoplasma *254*, 1187–1199.

Tas, R.P., Chazeau, A., Cloin, B.M.C., Lambers, M.L.A., Hoogenraad, C.C., and Kapitein, L.C. (2017). Differentiation between oppositely oriented microtubules controls polarized neuronal transport. Neuron *96*, 1264–1271.e5.

Uehara, R., Nozawa, R.S., Tomioka, A., Petry, S., Vale, R.D., Obuse, C., and Goshima, G. (2009). The augmin complex plays a critical role in spindle microtubule generation for mitotic progression and cytokinesis in human cells. Proc. Natl. Acad. Sci. U S A *106*, 6998–7003.

van Beuningen, S.F.B., Will, L., Harterink, M., Chazeau, A., van Battum, E.Y., Frias, C.P., Franker, M.A.M., Katrukha, E.A., Stucchi, R., Vocking, K., et al. (2015). TRIM46 controls neuronal polarity and axon specification by driving the formation of parallel microtubule arrays. Neuron *88*, 1208–1226.

Witte, H., Neukirchen, D., and Bradke, F. (2008). Microtubule stabilization specifies initial neuronal polarization. J. Cell Biol. *180*, 619–632.

Yalgin, C., Ebrahimi, S., Delandre, C., Yoong, L.F., Akimoto, S., Tran, H., Amikura, R., Spokony, R., Torben-Nielsen, B., White, K.P., and Moore, A.W. (2015). Centrosomin represses dendrite branching by orienting microtubule nucleation. Nat. Neurosci. *18*, 1437–1445.

Yau, K.W., van Beuningen, S.F., Cunha-Ferreira, I., Cloin, B.M., van Battum, E.Y., Will, L., Schätzle, P., Tas, R.P., van Krugten, J., Katrukha, E.A., et al. (2014). Microtubule minus-end binding protein CAMSAP2 controls axon specification and dendrite development. Neuron *82*, 1058–1073.

Yau, K.W., Schätzle, P., Tortosa, E., Pagès, S., Holtmaat, A., Kapitein, L.C., and Hoogenraad, C.C. (2016). Dendrites in vitro and in vivo contain microtubules of opposite polarity and axon formation correlates with uniform plus-end-out microtubule orientation. J. Neurosci. *36*, 1071–1085.

Zhou, W., Chang, J., Wang, X., Savelieff, M.G., Zhao, Y., Ke, S., and Ye, B. (2014). GM130 is required for compartmental organization of dendritic Golgi outposts. Curr. Biol. *24*, 1227–1233.

Cell Reports, Volume *24*

Supplemental Information

The HAUS Complex Is a Key Regulator of Non-centrosomal Microtubule Organization during Neuronal Development

Inês Cunha-Ferreira, Anaël Chazeau, Robin R. Buijs, Riccardo Stucchi, Lena Will, Xingxiu Pan, Youri Adolfs, Christiaan van der Meer, Joanna C. Wolthuis, Olga I. Kahn, Philipp Schätzle, Maarten Altelaar, R. Jeroen Pasterkamp, Lukas C. Kapitein, and Casper C. Hoogenraad

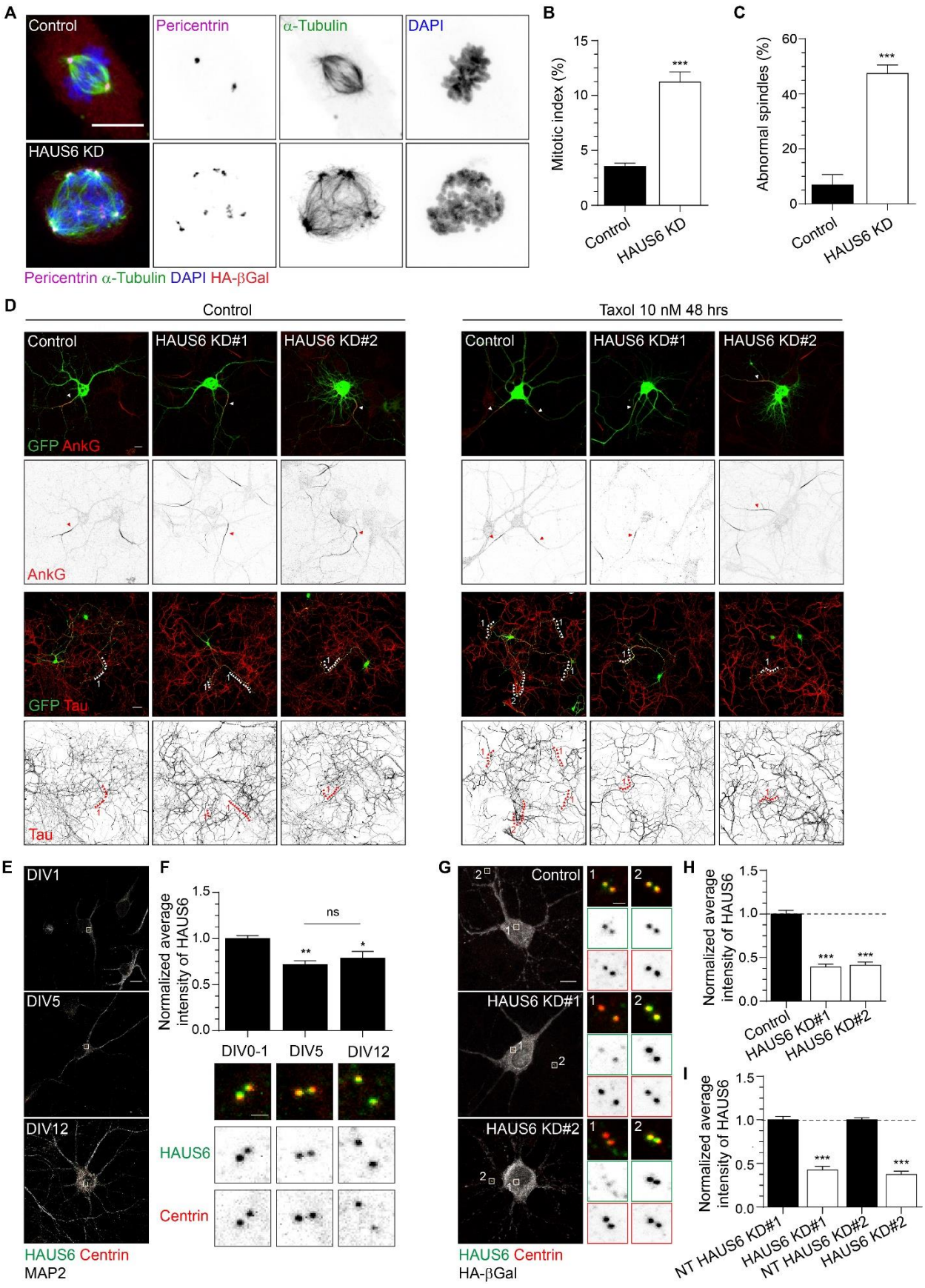
A
Control
Pericentrin
α-Tubulin
DAPI
HAUS6 KD
Pericentrin α-Tubulin DAPI HA-βGal
B
Mitotic index (%)
15
10
5
0
***
Control
HAUS6 KD
C
Abnormal spindles (%)
60
40
20
0
***
Control
HAUS6 KD
D
Control
Taxol 10 nM 48 hrs
Control
HAUS6 KD#1
HAUS6 KD#2
GFP AnkG
AnkG
GFP Tau
Tau
E
DIV1
DIV5
DIV12
HAUS6 Centrin
MAP2
F
Normalized average intensity of HAUS6
1.5
1.0
0.5
0.0
ns
**
*
DIV0-1
DIV5
DIV12
HAUS6
Centrin
G
Control
HAUS6 KD#1
HAUS6 KD#2
HAUS6 Centrin
HA-βGal
H
Normalized average intensity of HAUS6
1.5
1.0
0.5
0.0
***
***
Control
HAUS6 KD#1
HAUS6 KD#2
I
Normalized average intensity of HAUS6
1.5
1.0
0.5
0.0
***
***
NT HAUS6 KD#1
HAUS6 KD#1
NT HAUS6 KD#2
HAUS6 KD#2

Figure S1. The HAUS Complex is required for Neuronal Migration and Axon Specification, Related to Figure 1.

(A) Maximum intensity projection of IMCD3 murine mitotic cells depleted of HAUS6 and pSuper control. Pericentrin (magenta), α-Tubulin (green), HA-β-galactosidase (red), DAPI (blue).

(B, C) Mitotic index (B) and percentage of abnormal mitotic spindles (C) after depletion of HAUS6 and pSuper control in IMCD3 cells (n=922-1206 in B, n=82-142 in C, N=3).

(D) DIV6 hippocampal neurons co-transfected with GFP and shRNAs for pSuper control, HAUS6 KD#1,2 at DIV2 and treated at DIV4 with control vehicle (DMSO) or Taxol. GFP (green) and AnkG or Tau (red). Processes positive for AnkG or Tau are indicated white arrowheads in merged images and red in gray-scale inverted images. Tau positive axons are numbered.

(E) Maximum intensity projections of DIV1, DIV5 and DIV12 hippocampal neurons labelled with HAUS6 (green), Centrin (red), MAP2 (gray).

(F) Normalized average intensity of HAUS6 at the centrosome in DIV0-1, DIV5 and DIV12 hippocampal neurons. Data normalized to DIV0-1 stage of development (n=23-24, N=2). Insets in F depict indicated areas in E.

(G) Maximum intensity projections of hippocampal neurons at DIV12 co-transfected with HA-β-galactosidase and shRNAs for HAUS6 KD#1, 2 or pSuper control. HAUS6 (green), Centrin (red), HA-β-galactosidase (gray). Inset #1 highlights the centrosome in a transfected cell and inset #2, the centrosome in a non-transfected cell.

(H, I) Normalized average intensity of HAUS6 related to G. Data was normalized to pSuper control in H (n=28-29, N=3) and to non-transfected cells (NT) within the same coverslip in I (n=28-30, N=3).

Graphs represent mean±SEM. *p<0.05, **p<0.01, ***p<0.001. Scale bar 10 μm in A, E, G, 1 μm in F, G (centrosome panels), 10 μm in AnkG panels and 50 μm in Tau panels in D.

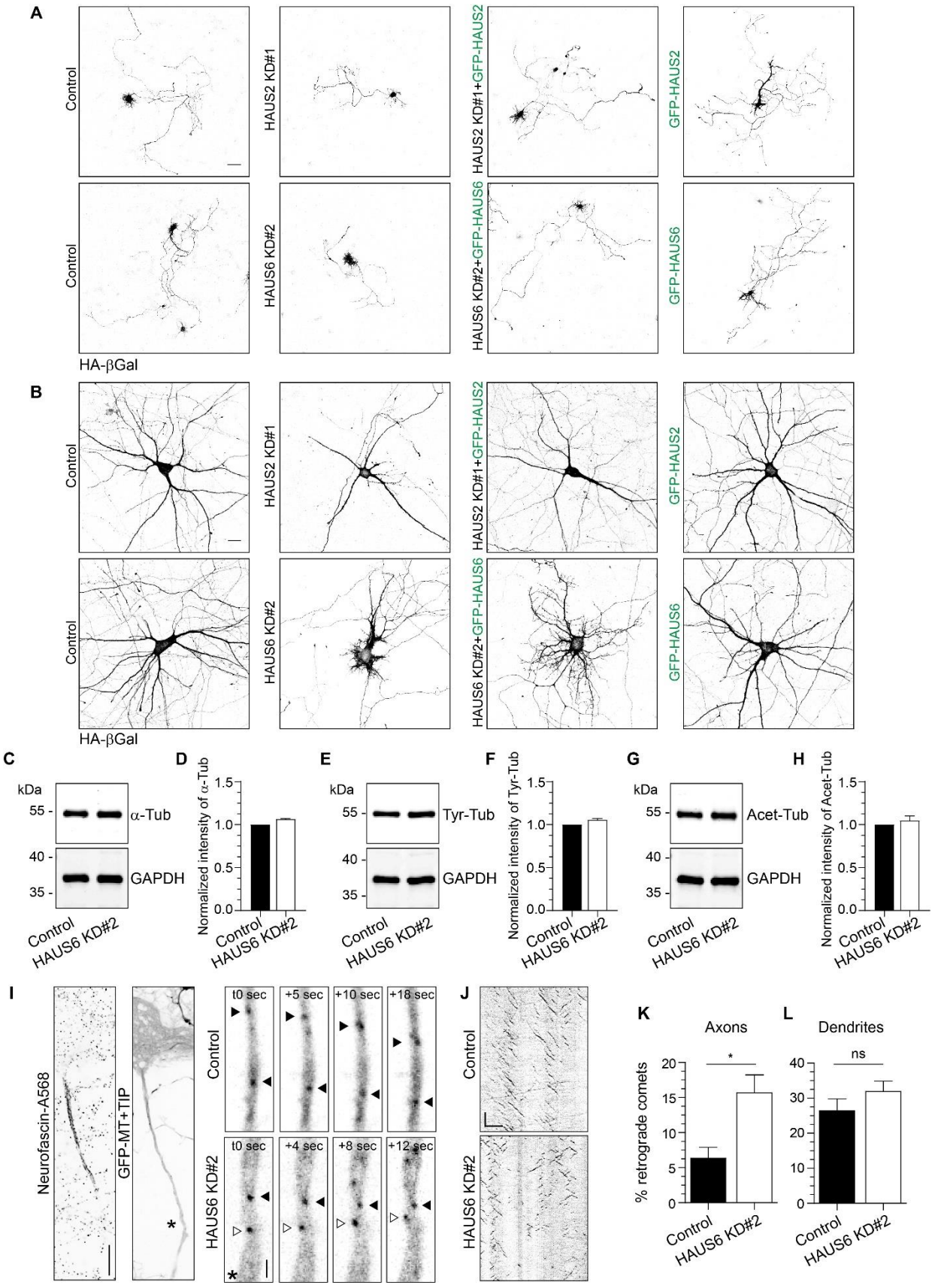
A
Control
HAUS2 KD#1
HAUS2 KD#1+GFP-HAUS2
GFP-HAUS2
Control
HAUS6 KD#2
HAUS6 KD#2+GFP-HAUS6
GFP-HAUS6
HA-βGal
B
Control
HAUS2 KD#1
HAUS2 KD#1+GFP-HAUS2
GFP-HAUS2
Control
HAUS6 KD#2
HAUS6 KD#2+GFP-HAUS6
GFP-HAUS6
HA-βGal
C
kDa
55
α-Tub
40
GAPDH
35
Control
HAUS6 KD#2
D
Normalized intensity of α-Tub
1.5
1.0
0.5
0.0
Control
HAUS6 KD#2
E
kDa
55
Tyr-Tub
40
GAPDH
35
Control
HAUS6 KD#2
F
Normalized intensity of Tyr-Tub
1.5
1.0
0.5
0.0
Control
HAUS6 KD#2
G
kDa
55
Acet-Tub
40
GAPDH
35
Control
HAUS6 KD#2
H
Normalized intensity of Acet-Tub
1.5
1.0
0.5
0.0
Control
HAUS6 KD#2
I
Neurofascin-A568
GFP-MT+TIP
Control
t0 sec
+5 sec
+10 sec
+18 sec
HAUS6 KD#2
t0 sec
+4 sec
+8 sec
+12 sec
J
Control
HAUS6 KD#2
K
Axons
*
% retrograde comets
20
15
10
5
0
Control
HAUS6 KD#2
L
Dendrites
ns
40
30
20
10
0
Control
HAUS6 KD#2

Figure S2. The HAUS Complex is Required for Neuronal Development and Microtubule Organization in Hippocampal Neurons, Related to Figure 2 and 3.

(A, B) Images of DIV5 (A) and DIV12 (B) hippocampal neurons co-transfected with HA-β-galactosidase and pSuper control, HAUS2 KD#1 or HAUS6 KD#2 with GFP, GFP-HAUS2 or GFP HAUS6 (shRNA resistant).

(C-H) Cortical neurons electroporated with pSuper control and HAUS6 KD#2 shRNAs were analysed by western blot with α-Tubulin (C, D), tyrosinated tubulin (E, F), acetylated tubulin (G, H) and GAPDH antibodies (loading control). Quantification of normalized levels of α-Tubulin, tyrosinated tubulin and acetylated tubulin to the Control is shown in D, F and H respectively (N=2).

(I, J) Representative stills and kymographs of GFP-MT+TIP from 10 minute time lapse acquisitions of DIV11 neurons transfected with pSuper control and HAUS6 KD#2 shRNAs. Time is in seconds. Anterograde and retrograde growing MT+TIPs are indicated with black and white arrowheads, respectively. Extracellular labelling with Neurofascin-Alexa568 is used as an axon marker.

(K, L) Percentage of retrograde comets from data in I, J (n=16-30, N=4-5 in K and n=20-33, N=3 in L).

Graphs represent the mean±SEM. *$p<0.05$. Scale bar 50 μm in A, 20 μm in B, 10 μm in panels and 1 μm in stills in I, 5 μm and 1 minute in J.

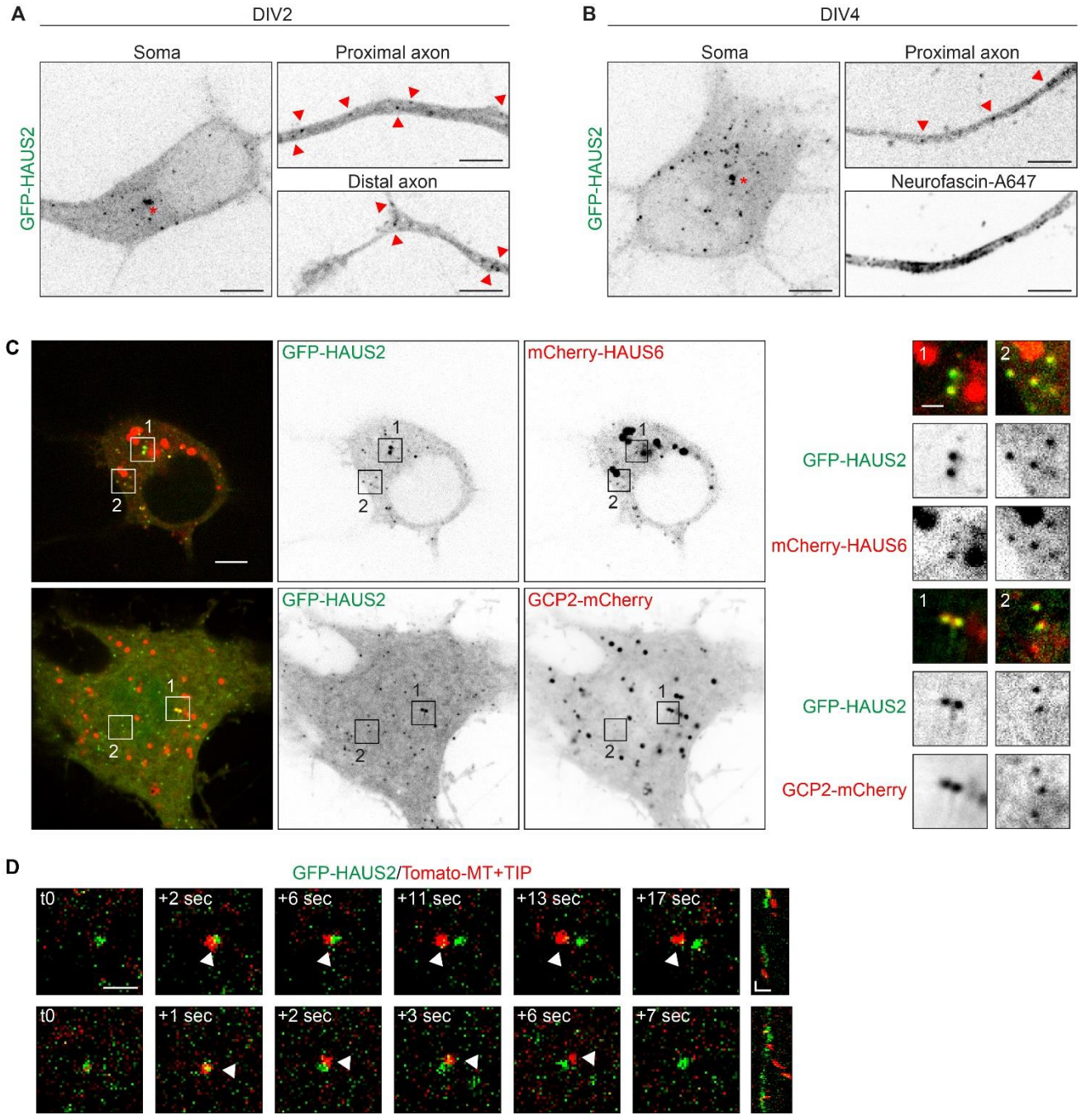

Figure S3. Localization of GFP-HAUS2, HAUS6-mcherry and GCP2-mcherry in Hippocampal Neurons, Related to Figure 4.

(A) Maximum intensity projection of a DIV2 neuron expressing GFP-HAUS2. The localization of GFP-HAUS2 clusters in proximal and distal axon is depicted in average projections of 10 frame acquisitions. GFP-HAUS2 localization at the centrosome is indicated with an asterisk and at non-centrosomal clusters along the axon with red arrowheads.

(B) Maximum intensity projection of a DIV4 neuron expressing GFP-HAUS2. The localization of GFP-HAUS2 clusters in proximal axon is depicted in average projections of 10 frame acquisitions. GFP-HAUS2 localization at the centrosome is depicted with an asterisk and non-centrosomal clusters along the axon with red arrowheads. Extracellular labelling with Neurofascin-Alexa647 was used as an axon marker.

(C) Average intensity projections of 10 frame stream acquisition of DIV10 hippocampal neurons co-transfected with GFP-HAUS2 (green) and mCherry-HAUS6 or GCP2-mCherry (red). Inset #1 indicates the centrosome and inset #2 the clusters outside the centrosome.
(D) Kymographs of 10 minute time lapse acquisitions of DIV17 neurons co-transfected with GFP-HAUS2 (green) and Tomato-MT+TIP (red).
Scale bar 5 μm in A, B, 5 μm in panels and 1 μm in insets in C, 1 μm in stills and 1 μm and 10 s in kymographs in D.

A

Accession	Description	Bio-GFP		Bio-GFP-HAUS2		Bio-GFP-HAUS6	
		#Peptides	#PSM	#Peptides	#PSM	#Peptides	#PSM
Q96CS2	HAUS1			6	7	6	7
Q9NVX0	HAUS2			21	235	5	7
Q68CZ6	HAUS3			14	19	10	17
Q9H6D7	HAUS4			15	24	6	9
O94927	HAUS5			22	36	20	28
Q7Z4H7	HAUS6			14	22	54	306
Q99871	HAUS7			7	14	6	13
Q9BT25	HAUS8			4	4	5	6

B

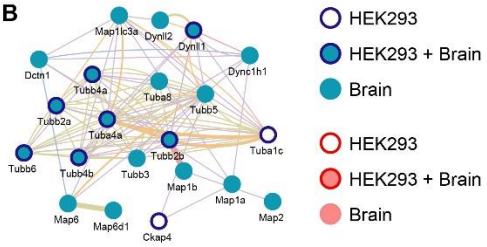

C

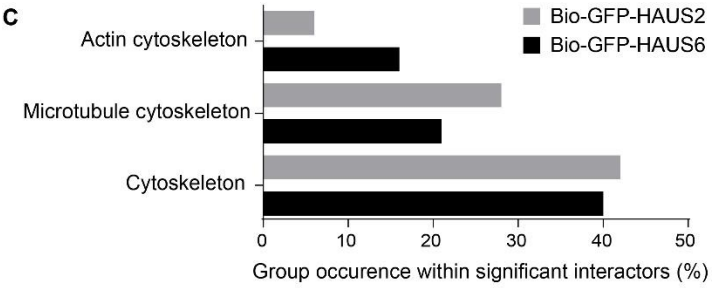

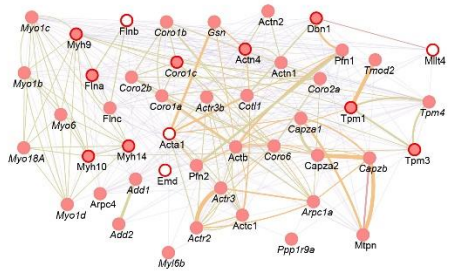

D

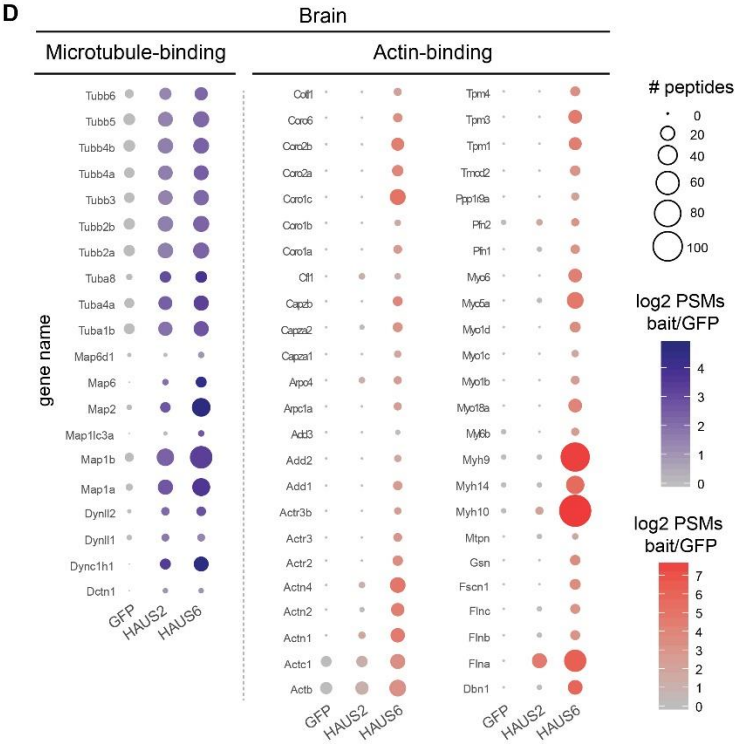

E

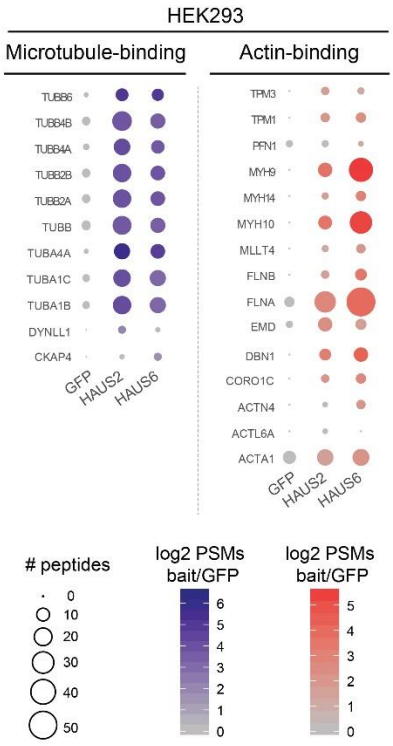

F

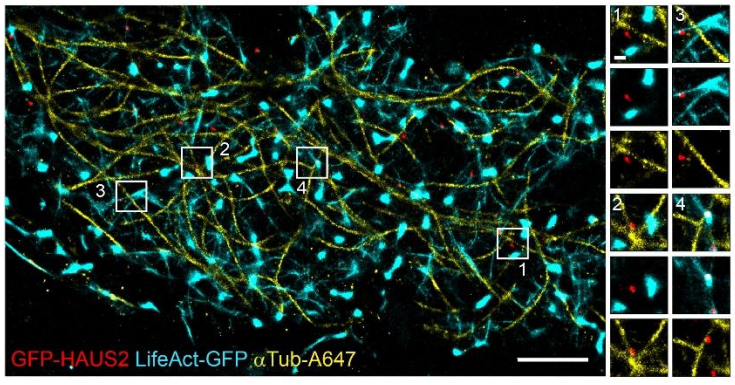

G

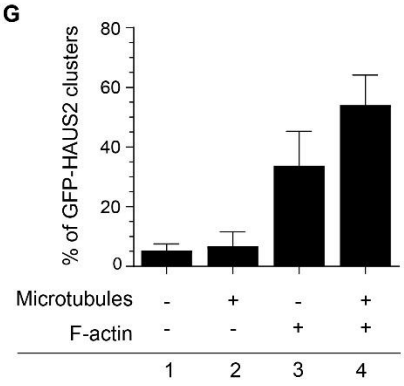

Figure S4. HAUS2 and HAUS6 Interact with Microtubule and Actin Binding Proteins in Brain, Related to Figure 4.
(A) HAUS binding partners of Bio-GFP-HAUS2 and HAUS6 in HEK293 cells identified by AP-MS.
(B) Network analysis on HAUS2 and 6 putative binding partners associated with the microtubule (blue) and actin cytoskeleton (red). Edge color coding: blue, colocalization; orange, predicted interaction; green, shared protein domain; purple, co-expression.
(C) Subset of Gene Ontology classifiers (actin cytoskeleton, microtubule cytoskeleton and cytoskeleton) overrepresented in HAUS2 (grey) or HAUS6 (black) significant interactors in adult rat bains.
(D, E) Selected putative binding partners of Bio-GFP-HAUS2 and HAUS6 identified in adult rat brains (D) and HEK293 (E) by AP-MS. The peptide count is graphically represented by spheres, the ratio of the spectral counts of the bait over the control is represented in blue for microtubule binding proteins and red for actin binding proteins.
(F) Single molecule super-resolution reconstruction of a DIV4 hippocampal neuron transfected with GFP-HAUS2 (red), extracted and fixed with GA and PFA, and post-labelled with LifeAct-GFP (cyan) and DNA-PAINT (yellow) to visualize actin and α-Tubulin, respectively. Insets depict indicated areas.
(G) Percentage of GFP-HAUS2 clusters across 4 different categories: 1 – No colocalization, 2 – colocalization with microtubules, 3 – colocalization with actin and 4 – colocalization with microtubules and actin. (n=3, N=1).
Data is presented as mean±SD. Scale bar 2 μm in panel and 500 nm in insets in F.

Supplemental Tables

Table S1. Overview of the Data and Statistical Analysis in this Study, Related to Figure 1-4 and Figure S1, S2 and S4.

Figure	Sample size (n)	N	Statistical test	Values
1B	Control = 15 slices HAUS6 KD = 16 slices	6 (≥ 3litters) 6 (≥ 3litters)	Mann Whitney U test	Control x HAUS6 KD bin 20: U = 11, p = 0.3095 Control x HAUS6 KD bin 40: U = 5, p = 0.0411 Control x HAUS6 KD bin 60: U = 13, p = 0.4848 Control x HAUS6 KD bin 80: U = 8, p = 0.1320 Control x HAUS6 KD bin 100: U = 4, p = 0.0260
1D	Control = 5 slices (51 neurons) HAUS6 KD = 6 slices (92 neurons)	3 (2 litters) 3 (2 litters)	Mann Whitney U test	U = 0, p = 0.0043
1E	Control = 5 slices (51 neurons) HAUS6 KD = 6 slices (92 neurons)	3 (2 litters) 3 (2 litters)	Mann Whitney U test	U = 0, p = 0.0043
1F	Control = 5 slices (51 neurons) HAUS6 KD = 6 slices (92 neurons)	3 (2 litters) 3 (2 litters)	Mann Whitney U test	Type 1: U = 0, p = 0.0043 Type 2: U = 0, p = 0.0043 Type 3: U = 1.500, p = 0.0108 Type 4: U = 4, p = 0.0498
1H	Control TRIM46 = 32 Control AnkG = 34 Control Tau = 19 HAUS6 KD#1TRIM46 = 32 HAUS6 KD#1 AnkG = 34 HAUS6 KD#1 Tau = 21 HAUS6 KD#2 TRIM46 = 32 HAUS6 KD#2 AnkG = 34 HAUS6 KD#2 Tau = 22	3 3 2 3 3 2 3 3 2	Kruskal-Wallis test Dunn's multiple comparisons test	Kruskal-Wallis test H (χ^2) = 8.993; p = 0.3429 Dunn's multiple comparisons test TRIM46 - Control x HAUS6 KD#1: p > 0.9999 TRIM46 - Control x HAUS6 KD#2: p > 0.9999 AnkG - Control x HAUS6 KD#1: p > 0.9999 AnkG - Control x HAUS6 KD#2: p > 0.9999 Tau - Control x HAUS6 KD#1: p > 0.9999 Tau - Control x HAUS6 KD#2: p > 0.9999
1I	Control TRIM46 = 31 Control AnkG = 34 Control Tau = 18 HAUS6 KD#1 TRIM46 = 30 HAUS6 KD#1 AnkG = 33 HAUS6 KD#1 Tau = 20 HAUS6 KD#2 TRIM46 = 31 HAUS6 KD#2 AnkG = 32 HAUS6 KD#2 Tau = 22	3 3 2 3 3 2 3 3 2	Kruskal-Wallis test Dunn's multiple comparisons test	Kruskal-Wallis test H (χ^2) = 84.88; p < 0.0001 Dunn's multiple comparisons test TRIM46 - Control x HAUS6 KD#1: p = 0.0029 TRIM46 - Control x HAUS6 KD#2: p < 0.0001 AnkG - Control x HAUS6 KD#1: p = 0.0003 AnkG - Control x HAUS6 KD#2: p < 0.0001 Tau - Control x HAUS6 KD#1: p = 0.0021 Tau - Control x HAUS6 KD#2: p < 0.0001
2B	Control = 19 γ-Tub KD = 20 HAUS2 KD#1 = 18 HAUS2 KD#2 = 20 HAUS6 KD#1 = 20 HAUS6 KD#2 = 20	2 2 2 2 2 2	One Way ANOVA Holm-Sidak's multiple comparisons test	One Way ANOVA F (DFn, DFd) = F (5, 111) = 17.59, p < 0.0001 Holm-Sidak's multiple comparisons test Control x γ-Tub KD: p < 0.0001 Control x HAUS2 KD#1: p < 0.0001 Control x HAUS2 KD#2: p < 0.0001 Control x HAUS6 KD#1: p < 0.0001

				Control x. HAUS6 KD#2: p < 0.0001
2C	Control = 24 GFP-HAUS2 = 20 HAUS2 KD#1 = 21 HAUS2 KD#1 + GFP-HAUS2 = 18	2 2 2 2	One Way ANOVA Holm-Sidak's multiple comparisons test	One Way ANOVA F (DFn, DFd) = F (3, 79) = 15.36, p < 0.0001 Holm-Sidak's multiple comparisons test Control x GFP-HAUS2: p = 0.2334 Control x HAUS2 KD#1: p < 0.0001 Control x HAUS2 KD#1 + GFP-HAUS2: p = 0.1556 GFP-HAUS2 x HAUS2 KD#1: p < 0.0001 GFP-HAUS2 x HAUS2 KD#1 + GFP-HAUS2: p = 0.0184 HAUS2 KD#1 x HAUS2 KD#1 + GFP-HAUS2: p = 0.0064
2D	Control = 21 GFP-HAUS6 = 19 HAUS6 KD#2 = 20 HAUS6 KD#2 + GFP-HAUS6 = 22	2 2 2 2	One Way ANOVA Holm-Sidak's multiple comparisons test	One Way ANOVA F (DFn, DFd) = F (3, 78) = 18.68, p < 0.0001 Holm-Sidak's multiple comparisons test Control x GFP-HAUS6: p = 0.4121 Control x HAUS6 KD#2: p < 0.0001 Control x HAUS6 KD#2 + GFP-HAUS6: p = 0.1387 GFP-HAUS6 x HAUS6 KD#2: p < 0.0001 GFP-HAUS6 x HAUS6 KD#2 + GFP-HAUS6: p = 0.0321 HAUS6 KD#2 x HAUS6 KD#2 + GFP-HAUS6: p = 0.0001
2F,G	Control = 46 γ-Tubulin = 46 HAUS2 KD#1 = 20 HAUS2 KD#2 = 23 HAUS6 KD#1 = 20 HAUS6 KD#2 = 22	2 2 2 2 2 2		
2H	Control = 20 GFP-HAUS2 = 20 HAUS2 KD#1 = 20 HAUS2 KD#1 + GFP-HAUS2 = 20	2 2 2 2		
2I	Control = 30 GFP-HAUS6 = 30 HAUS6 KD#2 = 30 HAUS6 KD#2 + GFP-HAUS6 = 30	3 3 3 3		
2J	Control = 46 γ-Tubulin = 46 HAUS2 KD#1 = 20 HAUS2 KD#2 = 23 HAUS6 KD#1 = 20 HAUS6 KD#2 = 22	2 2 2 2 2 2	Two Way ANOVA Dunnett's multiple comparisons test	Two Way ANOVA Interaction: F (DFn, DFd) = F (50, 1881) = 2.991, p < 0.0001 Distance: F (DFn, DFd) = F (10, 1881) = 55.47, p < 0.0001 Sample: F (DFn, DFd) = F (5, 1881) = 38.05, p < 0.0001 Dunnett's multiple comparisons test Control x γ-Tubulin: p < 0.0001 Control x HAUS2_KD#1: p < 0.0001 Control x HAUS2_KD#2: p < 0.0001 Control x HAUS6_KD#1: p = 0.0368 Control x HAUS6_KD#2: p < 0.0001
2K	Control = 20 HAUS2 KD#1 = 20 GFP-HAUS2 = 20 HAUS2 KD#1 + GFP-HAUS2 = 20	2 2 2 2	Two Way ANOVA Tukey's multiple comparisons test	Two Way ANOVA Interaction: F (DFn, DFd) = F (30, 836) = 1.751, p = 0.0080 Distance: F (DFn, DFd) = F (10, 836) = 20.06, p < 0.0001 Sample: F (DFn, DFd) = F (3, 836) = 104.1, p < 0.0001 Tukey's multiple comparisons test Control x HAUS2 KD#1: p < 0.0001 Control x GFP-HAUS2: p = 0.9912 Control x HAUS2 KD#1 + GFP-HAUS2: p = 0.0281 HAUS2 KD#1 x GFP-HAUS2: p < 0.0001 HAUS2 KD#1 x HAUS2 KD#1 + GFP-HAUS2: p = 0.0026 GFP-HAUS2 x HAUS2 KD#1 + GFP-HAUS2: p = 0.0620
2L	Control = 30 HAUS6 KD#2 = 30 GFP-HAUS6 = 30 HAUS6 KD#2 + GFP-HAUS6 = 30	3 3 3 3	Two Way ANOVA Tukey's multiple comparisons test	Two Way ANOVA Interaction: F (DFn, DFd) = F (30, 1276) = 15.97, p < 0.0001 Distance: F (DFn, DFd) = F (10, 1276) = 38.29, p < 0.0001 Sample: F (DFn, DFd) = F (3, 1276) = 35.20, p < 0.0001 Tukey's multiple comparisons test Control x HAUS6 KD#2: p = 0.0009 Control x GFP-HAUS6: p = 0.3251 Control x HAUS6 KD#2 + GFP-HAUS6: p = 0.9813 HAUS6 KD#2 x GFP-HAUS6: p = 0.1562 HAUS6 KD#2 x HAUS6 KD#2 + GFP-HAUS6: p = 0.0002 GFP-HAUS6 x HAUS6 KD#2 + GFP-HAUS6: p = 0.1608
3B	Control = 20 HAUS6 KD#2 = 20	2 2	Two tailed unpaired t-test	t = 5.808, df = 38, p < 0.0001

3C	Control = 20 HAUS6 KD#2 = 20	2 2	Mann Whitney U test	U = 78, p = 0.0007
3E	Control = 17 HAUS6 KD#2 = 17	2 2	Two tailed unpaired t-test	t = 3.209, df = 32, p = 0.0030
3G	Control = 19 HAUS6 KD#2 = 17	2 2	Mann Whitney U test	U = 92.50, p = 0.0281
3H	Control = 19 HAUS6 KD#2 = 17	2 2	Two tailed unpaired t-test	t = 3.619, df = 34, p = 0.0010
4B	GFP-HAUS2/mCherry-HAUS6 = 28 GFP-HAUS2/GCP2-mCherry = 51	4 4		
4D	Control = 43 HAUS6 KD#2 = 43	2 2	Mann Whitney U test	U = 488, p = 0.0001
4G	GFP-HAUS2 = 23 neurons, 24 dendrites (485 events)	3	Two tailed unpaired t-test	t = 12.95, df = 46, p < 0.0001
4H	GFP-HAUS2 = 21 neurons, 22 dendrites (129 events)	3	Two tailed unpaired t-test	t = 0.1418, df = 42, p = 0.8879
4I	GFP-HAUS2 = 21 neurons, 22 dendrites (129 events)	3		
4J	GFP-HAUS2 = 21 neurons, 22 dendrites (129 events)	3		
S1B	Control = 1206 HAUS6 KD = 922	3 3	Two-tailed Chi-square with Yates' correction	χ^2, df (46.40, 1), p < 0.0001
S1C	Control = 82 HAUS6 KD = 142	3 3	Two-tailed Fisher's exact test	p < 0.0001
S1F	DIV0-1 = 23 DIV5 = 24 DIV12 = 24	2 2 2	One Way ANOVA Tukey's multiple comparisons test	One Way ANOVA F (DFn, DFd) = F (2, 68) = 7.664, p = 0.0010 Tukey's multiple comparisons test DIV0-1 x DIV5: p = 0.0010 DIV0-1 x DIV12: p = 0.0158 DIV5 x DIV12: p = 0.6264
S1H	Control = 29 HAUS6 KD#1 = 28 HAUS6 KD#2 = 29	3 3 3	One-way ANOVA Dunnett's multiple comparisons test	One Way ANOVA F (DFn, DFd) = F (2, 83) = 79.86, p < 0.0001 Dunnett's multiple comparisons test Control x HAUS6 KD#1: p < 0.0001 Control x HAUS6 KD#2: p < 0.0001
S1I	NT HAUS6 KD#1 = 30 HAUS6 KD#1 = 28 NT HAUS6 KD#2 = 30 HAUS6 KD#2 = 29	3 3 3 3	One-way ANOVA Sidak's multiple comparisons test	One-way ANOVA F (DFn, DFd) = F (3, 113) = 89.42, p < 0.0001 Sidak's multiple comparisons test NT HAUS6 KD#1 x HAUS6 KD#1: p < 0.0001 NT HAUS6 KD#2 x HAUS6 KD#2: p < 0.0001
S2D,F,H		2		
S2K	Control = 16 HAUS6 KD#2 = 30	4 5	Mann Whitney U test	U = 138, p = 0.0175
S2L	Control = 20 HAUS6 KD#2 = 33	3 3	Two tailed unpaired t-test	t = 1.200, df=51, p = 0.2357
S4G	3	1		

Supplemental Experimental Procedures

Further information and requests for resources and reagents should be directed to and will be fulfilled by the Lead Contact Casper Hoogenraad (c.hoogenraad@uu.nl).

Animals
All experiments were approved by the Dutch Animal Experiments Committee (Dier Experimenten Commissie [DEC]), performed in line with institutional guidelines of University Utrecht and UMC (University Medical Center) Utrecht and conducted in agreement with Dutch law (*Wet op de Dierproeven*, 1996) and European regulations (Directive 2010/63/EU). Female pregnant C57BL/6J mice were obtained from The Jackson Laboratory and female pregnant Wistar rats from Janvier. Both species were aged at least 10 weeks at the time of delivery. Upon delivery, mice and rats were kept in a controlled 12 hrs light-dark cycle with a temperature of 22 ± 1°C and were given unrestricted access to food and water. The animals were housed with companions in transparent plexiglas cages with wood-chip bedding and paper tissue for nest building and cage enrichment. For *in utero* electroporation experiments, embryos of both genders were used at E14.5 stage of development. For hippocampal and cortical neuron culture experiments obtained from rat embryos, embryos of both genders at E18 stage of development were used. None of the parameters analysed in this study are reported to be affected by embryo gender. The animals, pregnant females and embryos have not been involved in previous procedures.

Cell lines
HEK293 female cells (CRL1573) and mouse inner medullary collecting duct 3 (IMCD3) cells (CRL2123) were purchased from American Type Culture Collection (ATCC). The sex is undetermined for the IMCD3 cell line. Cell lines were not authenticated by authors after purchase. Both cell lines were cultured in DMEM/Ham's F10 (45%/45%) supplemented with 10% FCS and 1% penicillin/streptomycin at 37°C and 5% CO_2 and seeded on 18 mm glass coverslips prior to transfection, or in 10 cm dishes for biochemistry experiments.

Primary neuronal cultures, transfection and electroporation
Primary hippocampal and cortical cultures were prepared from E18 rat brains (both genders) by mechanical and enzymatic dissociation (Goslin and Banker, 1989; Kapitein et al., 2010b). Hippocampal neurons were plated on coverslips coated with poly-L-lysine (37.5 μg/mL, Sigma) and laminin (1.25 μg/mL, Roche Diagnostics) at a density of 100,000 cells/well. Hippocampal neurons were transfected using Lipofectamine 2000 (Invitrogen). Briefly, DNA (1.8 μg/well in a 12 well plate) was mixed with 3.3 μL of Lipofectamine 2000 in 200 μL NB, incubated for 30 minutes, and then added to the neurons in NB with 0.5 mM glutamine at 37°C in 5% CO_2 for 45 minutes to 1 hr. Next, neurons were washed with NB and transferred in the original medium at 37°C in 5% CO_2 for 24-48 hrs (for overexpression) or 96 hrs (for shRNA expression).
Primary cortical neurons were electroporated ($1{,}2x10^6$ cells per sample) using the Amaxa Rat Neuron Nucleofector kit (Lonza) with 3μg of DNA and plated in 6-well plates. Cells were grown at 37°C in 5% CO2 for 96 hrs prior to western blot analysis. Hippocampal and cortical neurons were cultured in Neurobasal medium (NB, GIBCO) supplemented with 2% B27 (GIBCO), 0.5 mM glutamine (GIBCO), 15.6 μM glutamate (Sigma-Aldrich) and 1% penicillin–streptomycin (GIBCO).

***In utero* electroporation**
In utero electroporation was performed as described previously (van Beuningen et al., 2015). Briefly, pregnant C57BL/6J mice were anaesthetized with Isoflurane (induction: 3-4%, surgery: 1.5-2%) at E14.5 and injected with 0.05 mg/kg buprenorfinhydrochloride in saline. The abdominal cavity was opened under sterile surgical conditions and uterine horns were exposed. 1.7 μL DNA mixture containing 0.6 μg/μL pSuper vector as control or a mix of two mouse HAUS6 shRNAs and 0.4 μg/μL GFP vector dissolved in MilliQ water with 0.05% Fast Green (Sigma) was injected in the lateral ventricles of the embryo using glass micro-pipettes (Harvard Apparatus) and a PLI-100 Picoinjector (Harvard Apparatus). Brains (motor cortex) were electroporated with gold plated tweezer-electrodes (Fisher Scientific) using an ECM 830 Electro-Square-Porator (Harvard Apparatus) set to 5 unipolar pulses at 30V (95 ms interval and 50 ms pulse length). Embryos were placed back into the abdomen, and abdominal muscles and skin were sutured separately. Mother mice were awakened by releasing them from Isoflurane. The welfare of the mother mice was controlled daily. Embryonic brains were collected at E17.5 and processed for immunohistochemistry.

Heterologous cell culture and transfection
HEK293 cells were transfected with polyethylenimine (1 μg/μL) (PEI, Polysciences) and IMCD3 with Lipofectamine 2000 (Invitrogen) according to manufacturer's protocol. Coverslips with transfected IMCD3 cells were fixed and used for immunocytochemistry and HEK293 were processed for biochemistry experiments.

DNA and shRNA constructs
The following mammalian expression vectors have been described: pGW1 (Hoogenraad et al., 2005), pGW2 and pβactin (Kapitein et al., 2010a), pGW2-BFP (Tortosa et al., 2017), pβactin-HA-β-galactosidase (Hoogenraad et al., 2005), pSuper vector (Brummelkamp et al., 2002), Bio-GFP vector (Jaworski et al., 2009), BirA vector was a kind gift from Dr. D. Meijer

(Erasmus MC, Rotterdam, The Netherlands). p-Syn-TdTomato-MACF18 which we named Tomato-MT+TIP was used as a general marker of microtubule growing plus ends. Briefly, the vector was generated by replacing the CMV promoter and intron sequence of GW2 (MluI/HindIII) with the 0.5 kb rat Synapsin promoter (Dittgen et al., 2004). Tomato-MACF18 is identical to GFP-MACF18 (Schatzle et al., 2016) except for the exchange of GFP to tandem dimer Tomato. The GFP-MT+TIP construct used in live-imaging experiments to track polymerizing ends of microtubules was p-Syn-GFP-MACF18 (with Synapsin promoter) generated using published strategy to reduce expression levels, since we used it in conjunction with shRNA expressed for 96 hrs (Ferreira et al., 2013). Upstream open reading frame containing a Kozak sequence was introduced before the start codon of GFP in the synGFP-MACF18 construct. Depending on Kozak sequence strength, a certain percent of the ribosomes are expected to initiate translation here and disassemble once they reach the stop codon, therefore the number of ribosomes that can translate the gene of interest is lowered and expression becomes significantly reduced. The Kozak sequence used was gggATGGGTTAAGGCCTaccATG. pGW2-GFP, pGW2-mRFP and pGW2-mCherry were created by inserting each tag in HindIII/AscI sites of a pGW2 vector. Full length human HAUS2 RefSeq 235 aa isoform (NCBI:NM_018097.2, UniProt:Q9NVX0) was amplified by PCR from pEGFP-C1-HAUS2 (a kind gift from Dr. Laurence Pelletier, Lunenfeld-Tanenbaum Research Institute, Mount Sinai Hospital, Toronto, Canada) and inserted in AscI/SalI sites of pGW2-GFP expression vector. To generate pGW2-GFP-HAUS6 the full length RefSeq 955 aa isoform (NCBI:NM_017645, UniProt:Q7Z4H7) was amplified by PCR from pEGFP-C1-HAUS6 (a kind gift from Dr. Laurence Pelletier, Lunenfeld-Tanenbaum Research Institute, Mount Sinai Hospital, Toronto, Canada) and inserted in AscI/SalI restriction sites of pGW2-GFP vector. pGW2-mCherry-HAUS6 was generated by recloning HAUS6 from pGW2-GFP-HAUS6 with AscI/SalI restriction sites and ligation with pGW2-mCherry. One HAUS6 construct resistant to shRNA was used in rescue experiments. Briefly, two silent mutations were inserted at Lys123 (G369A) and Ile125 (T375C) by site-directed mutagenesis of pGW2-GFP-HAUS6 described above. To generate Bio-GFP-HAUS2 or HAUS6, HAUS2 and HAUS6 were recloned from pGW2-GFP-HAUS2/6 with AscI/SalI restriction enzymes and inserted in Bio-GFP vector. To generate pGW2-GCP2-mCherry, mCherry was first amplified by PCR and inserted C terminally in a pGW2 vector. Full length human GCP2 RefSeq 902 aa (NCBI:NM_006659.3, UniProt:Q9BSJ2) was amplified by PCR from pGW1-GCP2-GFP (a kind gift from Dr. Kah W. Yau and Dr. Kai Jiang, Department of Cell Biology, University of Utrecht, The Netherlands) and inserted upstream of mCherry in AscI/SalI restriction sites of pGW2-mCherry. The following shRNA constructs were created and used in this study: pSuper mouse HAUS6 shRNA#1 (5'-aggagagagacgttattag-3'), pSuper mouse HAUS6 shRNA#2 (5'-caggctttcagaaactagt -3'), pSuper rat HAUS2 shRNA#1 (HAUS2 KD#1) (5'-gaggagatgttagatatat-3'), pSuper rat HAUS2 shRNA#2 (HAUS2 KD#2) (5'-cgttcagtcaattacatgt-3'), pSuper rat HAUS6 shRNA#1 (HAUS6 KD#1) (5'-gggaaagattatcagatat -3'), pSuper rat HAUS6 shRNA#2 (HAUS6 KD#2) (5'- gtcctaagtttattcatct -3'). shRNA sequences were created with http://sirna.wi.mit.edu/ (Yuan et al., 2004) and oligonucleotides were annealed and inserted in pSuper vector (HindIII/BglII).

Antibodies and Reagents

The following antibodies were used in this study: chicken anti-β-galactosidase (Aves Labs BGL-1040, RRID:AB_2313507), chicken anti-MAP2 (Abcam, ab5392, RRID:AB_2138153), mouse anti-dephosphorylated Tau clone PC1C6 (Chemicon, MAB3420, RRID:AB_94855), mouse anti-Acetylated Tubulin (Sigma-Aldrich, T7451, RRID:AB_609894), mouse anti-Ankyrin G clone 4G3F8 (Life Technologies, 33-8800, RRID:AB_2533145), mouse anti-α-Tubulin (Sigma-Aldrich, T5168, RRID:AB_477579), mouse anti-Centrin clone 20H5 (Milipore, 04-1624, RRID:AB_11211820), mouse anti-HA clone 16B12 (Covance, MMS-101P-200, RRID:AB_10064068), mouse anti-MAP2 (Sigma-Aldrich, M9942, RRID:AB_477256), mouse anti-Pan-Neurofascin extracellular (UC Davis/NIH NeuroMab Facility, 75-172, RRID:AB_2282826), rabbit anti-Pericentrin (BioLegend, 923701, RRID:AB_2565440), rabbit anti-EB3 (02-1005-07, (Stepanova et al., 2003)), rabbit anti-GFP (MBL, 598, RRID:AB_591819), rabbit anti-HAUS6 (Uehara et al., 2009), rabbit anti-TRIM46 (van Beuningen et al., 2015), rat anti-Ctip2 (Abcam 18465, RRID:AB_2064130), rat anti-Tubulin Tyrosinated clone YL1/2 (Abcam, ab6160, RRID:AB_305328), rabbit anti-GAPDH (Sigma, G9545, RRID:AB_796208), anti-chicken IgY (IgG) Dyelight 405 (Jackson ImmunoResearch Labs, 703-475-155, RRID:AB_2340373), anti-chicken IgY Alexa568 (Life Technologies, A11041, RRID:AB_2534098), anti-mouse IgG Alexa488 (Life Technologies, A-11029, RRID:AB_2534088), anti-mouse IgG Alexa568 (Life Technologies, A11031, RRID:AB_144696), anti-mouse IgG Alexa647 (Life Technologies, A21236, RRID:AB_2535805), anti-mouse IgG2a Alexa 647 (Life Technologies, A-21241, RRID:AB_2535810), anti-mouse IgG2a Alexa594 (Life Technologies, A-21135, RRID:AB_2535774), anti-rabbit IgG Alexa488 (Life Technologies, A11034, RRID:AB_2576217), anti-rabbit IgG Alexa647 (Life Technologies, A21245, RRID:AB_2535813), anti-rat IgG Alexa488 (Life Technologies, A-11006, RRID:AB_2534074), anti-rat IgG Alexa568 (Life Technologies, A11077, RRID:AB_2534121), anti-mouse-D2 (Ultivue™-2 super-resolution 2-plex kit, U10001), anti-mouse IRDye800CW (Li-Cor/Westburg, 926-32210, RRID:AB_621842), anti-rat IRDye800CW (Li-Cor/Westburg, 926-32219, RRID:AB_1850025), anti-rabbit IRDye680LT rabbit (Li-Cor/Westburg, 926-68021, RRID:AB_10706309). Other reagents used in this study were: Lipofectamine 2000 (Thermofisher Scientific, 11668019), Polyethylenimine HCl MAX, Linear, MW 40000, Transfection Grade (PEI MAX 40K, Polysciences, 24765-2),

Taxol (Sigma-Aldrich, T7402), Vectashield mounting medium (Vector Labs, H-1000), Vectashield mounting medium with DAPI (Vector Labs, H-1200).

Immunofluorescence staining and imaging

For neuron immunocytochemistry cells were fixed for 10 minutes with paraformaldehyde (4%) or for 5 minutes with methanol (100%) at -20°C. Fixed neurons were washed 3 times for 5 minutes in PBS and incubated with primary antibodies in GDB buffer (0.2% BSA, 0.8 M NaCl, 0.5% Triton X-100, 30 mM phosphate buffer, pH 7.4) overnight at 4°C. After 3 times washing with PBS, cells were incubated with secondary antibodies in GDB buffer for 1 hr at room temperature. After washing, coverslips were mounted in Vectashield (VectorLabs) or mowiol. For methanol fixed samples, GDB was used without Triton. Live labelling of the axonal initial segment was performed with an antibody recognizing an extracellular epitope of neurofascin (Pan-Neurofascin extracellular (UC Davis/NIH NeuroMab Facility, 75-172, RRID:AB_2282826). Neurons were incubated with primary antibody in conditioned NB for 10 minutes, washed twice with fresh NB, incubated with a secondary Alexa-conjugated antibody for 8 minutes and washed twice with fresh NB. Extraction, fixation and immunocytochemistry for microtubules was performed as previously described (Chazeau et al., 2016). Briefly, cells were incubated for 90 seconds in extraction buffer preheated at 37°C (80 mM PIPES, 2 mM $MgCl_2$, 1 mM EGTA, 0.3% Triton-X100 and 0.25% glutaraldehyde, pH 6.9), followed by incubation with 4% PFA preheated at 37°C for 10 minutes. Neurons were further permeabilized with 0.25% Triton X-100 and blocking was performed with 2% w/v bovine serum albumin (BSA), 0.2% gelatin, 10 mM glycine, 50 mM NH_4Cl in PBS, pH 7.4. Primary and secondary antibodies were incubated for 1 hr at room temperature in blocking buffer. For SMLM (single-molecule localization microscopy), the same immunocytochemistry protocol was performed under the microscope using the secondary antibody anti-mouse-D2 and buffers from the Ultivue™-2 (super-resolution 2-plex kit). Cells with low expression levels of the different constructs were used in all the analysis. To visualize actin in SMLM, LifeAct-GFP was purified and used as a transient binding probe as previously described (Kiuchi et al., 2015; Tas et al., 2018).

Brain sections were obtained from embryos at E17.5 and fixed in 4% paraformaldehyde followed by submersion in 30% sucrose. Brains were placed in Jung tissue freezing medium (Leica) and cut in 12 µm coronal sections. Cryosections were blocked and permeabilized with 10% normal goat serum in 0.2% Triton X-100 PBS (Blocking buffer) for 1 hr followed by incubation with primary antibody diluted in blocking buffer overnight at 4°C. After washing, sections were incubated with secondary antibody diluted in blocking buffer for 90 minutes and mounted using Vectashield mounting medium containing DAPI (Vectorlabs).

IMCD3 cells were fixed for 5 minutes in methanol at -20°C. Fixed cells were washed 3 times in PBS following blocking and permeabilization with 2% BSA supplemented with 0.05% Tween-20 in PBS (Blocking buffer) for 20 minutes. Primary antibodies were diluted in blocking buffer and incubated overnight at 4°C. Secondary antibodies diluted in 0.05% Tween-20 in PBS (washing solution) were incubated with samples for 1 hr at room temperature after three rounds of washing. After washing 3 times in washing solution and a final wash in MilliQ, samples were mounted with Vectashield mounting medium with DAPI (Vectorlabs).

Imaging of fixed neurons or cell lines was performed using Confocal laser scanning microscopy with a Zeiss LSM700 confocal laser-scanning microscope with a Plan-Apochromat 63× N.A. 1.40 oil DIC, EC Plan-Neofluar 40× N.A. 1.30 Oil DIC and a Plan-Apochromat 20× N.A. 0.8 objective using 405 nm, 488 nm, 555 nm, and 633 nm laser lines. Confocal images of brain slices were acquired using a Zeiss LSM700 with a 20× N.A. 0.5 objective (for migration analysis) or a 40× N.A. 0.8 (for morphology analysis) using 405 nm, 488 nm, 555 nm, and 633 nm laser lines. A total thickness of 15 µm in 1 µm steps was scanned for each position, and maximum intensity projections were generated for analysis. To access the entire brain slice, four images were taken side by side and image stitching was performed using ZEN 2011 Software. The degree of neuronal migration was quantified as described previously (Hand et al., 2005).

Live imaging

Live imaging of neurons was performed using spinning-disk confocal microscopy with an inverted microscope Nikon Eclipse Ti-E incorporated with a Plan Apo VC 100× N.A. 1.40 oil objective, or a Nikon Eclipse TE2000E equipped with CFI Apo TIRF 100× N.A. 1.49; both microscopes are equipped with a Perfect Focus System, a Yokogawa CSU-X1-A1 spinning-disk confocal unit, an Evolve 512 EMCCD camera (Photometrics), and a motorized XYZ stage (Applied Scientific Instrumentation) which were all controlled using MetaMorph (Molecular Devices) software.

Three color SMLM was performed on a Nikon Ti microscope equipped with a 100× N.A. 1.49 Apo TIRF oil objective, a Perfect Focus System and an additional 2.5× Optovar to achieve an effective pixel size of 64 nm. Oblique laser illumination was achieved using a custom illumination pathway with a 15 mW 405 nm diode laser (Power Technology), a 50 mW 491 nm DPSS laser (Cobolt Calypso) and a 40 mW 640 nm diode laser (Power Technology). Fluorescence was detected using a water-cooled Andor DU-897D EMCCD camera and ET series Cy5 filter (Chroma Technology). All components were controlled by µManager software (Edelstein et al., 2010). After immunocytochemistry, samples were first incubated for 15

minutes with Tetraspeck™ 100 nm-beads (Invitrogen). High laser power induced blinking of GFP-HAUS2 was first imaged for 1000-2000 frames, after which it was completely bleached. LifeAct-GFP and fluorescently labelled DNA complementary strand, I2-650 (binding to anti-mouse-D2) were then added and diluted to obtain single molecule binding events. DNA-PAINT imaging was performed according to Ultivue™-2 super-resolution 2-plex kit protocol. Subsequently, LifeAct-GFP was imaged as previously described (Janssen et al., 2017). Between 20,000 and 30,000 frames were recorded per acquisition with exposure time of 100 ms.

Drug treatments
Where indicated, neurons were treated with 10 nM Taxol (Sigma) for 48 hrs.

Western blot
Cortical neuron lysates were prepared at DIV4 by scraping cells directly in sample buffer (4% SDS, 20% glycerol, 100 mM Tris pH 6.8, 200 mM DTT and 20 mg/l bromophenol blue). Samples were boiled at 99º C for 10 minutes and centrifuged at 16000 g before being analyzed by SDS-PAGE. Proteins were transferred to PVDF membranes (Millipore) using a wet blotting system (Bio-Rad). Membranes were blocked and incubated with primary antibodies (overnight at 4°C) in blocking buffer containing 3% BSA in PBS-T (PBS1x, 0.1% Tween-20). After three 10 minute washing steps in PBS-T membranes were incubated with secondary antibodies in blocking buffer for 1 hr at room temperature. Membranes were scanned using Odyssey infrared imaging system (Li-COR Biosciences). The relative intensities of α-, tyrosinated and acetylated tubulin were obtained by normalization to the GAPDH loading control. The relative intensity of each tubulin after HAUS6 knockdown was then normalized to the corresponding control. Quantifications were performed in Fiji (Schindelin et al., 2012).

Affinity Purification-Mass Spectrometry
Streptavidin beads pull-down assays were performed with HEK293 cells transfected with BirA and Bio-GFP-HAUS2, Bio-GFP-HAUS6 and Bio-GFP using polyethylenimine (PEI, Polysciences) for 48 hrs according to the manufacturer's instructions. Cells were lysed in RIPA lysis buffer (50 mM TrisHCl pH 7.4-7.8, 150 mM NaCl, 1% Triton X-100, 0.1% SDS, 0.5% Sodium Deoxycholate) and Protease inhibitors (Roche) for 30 minutes, centrifuged at 17949 g/rcf for 15 minutes at 4ºC and the supernatants incubated with Dynabeads M-280 blocked in chicken egg albumin (Life Technologies) for 1 hr at 4ºC. Beads were separated using a magnet rack (Dynal, Invitrogen) and washed five times in washing buffer (20 mM Tris-HCl pH 7.4-7.8, 150 mM KCl, 0.1% Triton X-100). Samples were collected at this point for AP-MS analysis of HEK293 cells expressing each construct. To sample for brain putative interactors of HAUS2 or HAUS6 pre-incubated Dynabeads with HEK293 cell extracts expressing each construct were washed twice in low salt washing buffer (20 mM Tris-HCl pH 7.4-7.8, 100 mM KCl, 0.1% Triton X-100), followed by two wash steps in high salt wash buffer (20 mM Tris-HCl pH 7.4-7.8, 500 mM KCl, 0.1% Triton X-100) and two final wash steps in low salt washing buffer to remove binding proteins from HEK293 cells. Brains were obtained from female adult rats and homogenized in 10x volume/weight in tissue lysis buffer (50 mM TrisHCl, 150 mM NaCl, 0.1% SDS, 0.2% NP-40, and protease inhibitors (Roche)). Brain lysates were centrifuged at 17494 g/rcf for 10 minutes at 4°C and the supernatant was incubated with the Dynabeads containing Bio-GFP-HAUS2, Bio-GFP-HAUS6 or Bio-GFP for 2 hrs at 4ºC and washed in wash buffer five times. For mass spectrometry analysis, beads were resuspended in 15 µL of 4x Laemmli sample buffer (Bio-Rad) and supernatants were loaded on a 4-12% gradient Criterion XT Bis-Tris precast gel (Bio-Rad). The gel was fixed with 40% methanol and 10% acetic acid and then stained for 1 hr using colloidal coomassie dye G-250 (Gel Code Blue Stain Reagent, Thermo Scientific). Each lane from the gel was cut in 3 slices, destained and digested using trypsin, as described previously (Ekkebus et al., 2013). Briefly, each lane from the gel was cut into three pieces and placed in 0.5-mL tubes. They were washed with 250 µL of water, followed by 15 minutes dehydration in acetonitrile. Proteins were reduced (10 mM dithiothreitol, 1 hr at 56°C), dehydrated and alkylated (55 mM iodoacetamide, 1 hr in the dark). After two rounds of dehydration, trypsin (Promega) was added to the samples (20 µL of 0.1 mg/mL trypsin in 50 mM Ammonium bicarbonate) and incubated overnight at 37°C. Peptides were extracted with acetonitrile, dried down and reconstituted in 10% formic acid prior mass spectrometry analysis.

Image analysis

No specific strategy for randomization and/or stratification was employed. The studies were blind in data analysis.

Quantification of immunofluorescence intensity
Images were acquired with a Zeiss LSM700 confocal microscope covering the entire neuron from top to bottom. Recording settings were kept the same for all conditions in each experiment. Only the planes that include the region of interest (ROI) were used for analysis. For quantification of signal intensity in dendrites ROIs within the first 10 µm were manually drawn in

proximal dendrites using Fiji (Schindelin et al., 2012). Mean intensity was measured from these regions and background values were subtracted. For quantification of signal intensity at the centrosome the mean intensity of HAUS6 at each centriole was quantified in average intensity projection images of selected planes by drawing ROIs of 0.3 μm radius encircling each centriole using Fiji. Background subtraction was performed by subtracting the mean intensity of the HAUS6 signal in the area juxtaposed to the centriole with ROIs of 0.3 μm radius from the mean intensity at the centriole. Quantification of HAUS6 at the centrosome for each neuron was obtained with the average of mean intensity of both centrioles.

Analysis of neuronal morphology

For analysis of axon development pβactin-GFP or pβactin-HA-β-galactosidase were used as a fill. The axon was identified based on morphology and the presence of AnkG marker in one neurite. Images were acquired with a Zeiss LSM700 confocal microscope. Only neurons with clearly defined neuronal arborisation were imaged and analysed. Total axonal length that includes the length of the longest branch and its branches was quantified with ImageJ software and NeuronJ plugin (Meijering et al., 2004). For analysis of dendritic development pβactin-GFP or pβactin-HA-β-galactosidase were used as a fill. The dendritic arbour was identified based on morphology, and the absence of AnkG marker used to label the axon. Images were acquired with a Zeiss LSM700 confocal microscope. Dendritic arbours were manually labelled in maximum intensity projection images using the Fiji plugin NeuronJ (Meijering et al., 2004). Analysis was performed based on the imported tracing data using the Sholl Analysis plugin v3.4.5 (Ferreira et al., 2014). The first circle was defined by the soma size and subsequent circles with increased 10 μm steps up to 100 μm distance from the cell body. Only branches longer than 8 μm were included in this analysis.

Quantification of EB3 comets

Images were acquired with a Zeiss LSM700 confocal microscope covering the entire neuron from top to bottom. Recording settings were kept the same for all conditions in each experiment. ROIs of approximately 10 μm long were manually drawn in proximal dendrites using Fiji (Schindelin et al., 2012). ImageJ plugin ComDet v.0.2.0 (GitHub: https://github.com/ekatrukha/ComDet) was used to quantify the number of EB3 comets in 10 μm proximal dendrites.

Colocalization and cluster analysis

Neurons expressing GFP-HAUS2 or GFP-HAUS2 with mCherry-HAUS6 or GCP2-mCherry (colocalization experiments) were imaged with spinning-disk confocal microscopy at 10 frames/second. Analysis of clusters was performed with the average intensity projection of 10 frames. GFP-HAUS2 clusters were quantified using the ImageJ plugin ComDet v.0.3.7 (GitHub: https://github.com/ekatrukha/ComDet). Numbers were normalized to the corresponding area. Colocalization was quantified as the percentage of mCherry-HAUS6 or GCP2-mCherry visually overlapping with GFP-HAUS2.

Quantification of moving clusters

Neurons expressing GFP-HAUS2 were imaged with spinning-disk confocal microscopy. Each neuron was imaged for 60 second at 5 frames/second. Run length, time and velocity of GFP-HAUS2 clusters were quantified from 60 second kymographs of proximal dendrites (25 μm) created using the Kymoreslicewide (GitHub: https://github.com/ekatrukha/KymoResliceWide) plugin with Fiji (Schindelin et al., 2012). The percentage of mobile *versus* immobile clusters was quantified in 20 second periods and averaged over a total of 60 seconds for each dendrite. The percentage of retrograde (to the soma) *versus* anterograde (to the dendrite) moving clusters was quantified over 60 second period for each dendrite.

Quantification of microtubule dynamics

GFP-MT+TIP marker was co-expressed with a HAUS6 shRNA (HAUS6 KD#2) or pSuper control for 96 hrs prior to spinning-disk confocal imaging. Each middle axon or dendrite (after a first or a second branch point) was imaged for 10 minutes at 1 frame/second. Recordings were low-pass filtered and subtracted with a sliding 10 frame average projection (Schatzle et al., 2016). Comet orientation was determined from a 10 minute kymograph created using the Kymoreslicewide (GitHub: https://github.com/ekatrukha/KymoResliceWide) plugin with Fiji (Schindelin et al., 2012). Starting and end positions of the traces were marked by the “Cell Counter” plugin, and coordinates were exported to determine the percentage of retrograde (to the soma) *versus* anterograde (to the dendrite or axon).

Quantification of mitotic defects

IMCD3 cells were imaged with a Zeiss LSM700 confocal microscope covering the cells from top to bottom. Cells in mitosis or with abnormal spindles were identified based on α-tubulin staining. The percentage of cells in mitosis (mitotic index) and the percentage of abnormal spindles were quantified in cells depleted for HAUS6 and compared with controls.

Mass spectrometry analysis
All samples were analysed on an Orbitrap Q-Exactive mass spectrometer (Thermo Fisher Scientific, Bremen, Germany) coupled to an Agilent 1290 Infinity LC (Agilent Technologies). Peptides were loaded onto a trap column (Reprosil C18, 3 µm, 2 cm × 100 µm; Dr. Maisch) with solvent A (0.1% formic acid in water) at a maximum pressure of 800 bar and chromatographically separated over the analytical column (Zorbax SB-C18, 1.8 µm, 40 cm × 50 µm; Agilent) using 90 min linear gradient from 7-30% solvent B (0.1% formic acid in acetonitrile) at a flow rate of 150 nL/min. The mass spectrometer was used in a data-dependent mode, which automatically switched between MS and MS/MS. After a survey scan from 350-1500 m/z the 10 most abundant peptides were subjected to HCD fragmentation. MS spectra were acquired in high-resolution mode (R > 30,000), whereas MS2 was in high-sensitivity mode (R > 15,000). For data analysis, raw files were processed using Proteome Discoverer 1.4 (version 1.4.1.14, Thermo Scientific, Bremen, Germany). Database searches were performed either using the human Uniprot database or the rat Uniprot database and Mascot (version 2.5.1, Matrix Science, UK) as the search engine. Carbamidomethylation of cysteines was set as a fixed modification and oxidation of methionine was set as a variable modification. Trypsin was set as cleavage specificity, allowing a maximum of 2 missed cleavages. Data filtering was performed using percolator, resulting in 1% false discovery rate (FDR). Additional filters were search engine rank 1 and mascot ion score >20.

Map of interactions analysis
Gene ontology (GO) classification was obtained via PANTHER (Mi et al., 2005). Selected HAUS2 and HAUS6 interactors linked to microtubule cytoskeleton or actin cytoskeleton were used for the generation of protein-protein interaction networks in Figure S4B. Network analyses were performed using the GeneMania plugin (Montojo et al., 2010) within Cytoscape (Shannon et al., 2003). Edge color coding: blue, colocalization; orange, predicted interaction; green, shared protein domain; purple, co-expression.

Gene ontology analysis
The percentage of occurrence of actin, microtubule cytoskeleton and cytoskeleton groups within the interactors of Bio-GFP-HAUS2 and HAUS6 was calculated. For the analysis the top 100-150 hits were selected and classified using g:Profiler (Reimand et al., 2016).

Supplemental References
Brummelkamp, T.R., Bernards, R., and Agami, R. (2002). A system for stable expression of short interfering RNAs in mammalian cells. Science (New York, NY) 296, 550-553.

Chazeau, A., Katrukha, E.A., Hoogenraad, C.C., and Kapitein, L.C. (2016). Studying neuronal microtubule organization and microtubule-associated proteins using single molecule localization microscopy. Methods Cell Biol 131, 127-149.

Dittgen, T., Nimmerjahn, A., Komai, S., Licznerski, P., Waters, J., Margrie, T.W., Helmchen, F., Denk, W., Brecht, M., and Osten, P. (2004). Lentivirus-based genetic manipulations of cortical neurons and their optical and electrophysiological monitoring in vivo. Proceedings of the National Academy of Sciences of the United States of America 101, 18206-18211.

Edelstein, A., Amodaj, N., Hoover, K., Vale, R., and Stuurman, N. (2010). Computer control of microscopes using microManager. Current protocols in molecular biology Chapter 14, Unit14.20.

Ekkebus, R., van Kasteren, S.I., Kulathu, Y., Scholten, A., Berlin, I., Geurink, P.P., de Jong, A., Goerdayal, S., Neefjes, J., Heck, A.J., *et al.* (2013). On terminal alkynes that can react with active-site cysteine nucleophiles in proteases. J Am Chem Soc 135, 2867-2870.

Ferreira, J.P., Overton, K.W., and Wang, C.L. (2013). Tuning gene expression with synthetic upstream open reading frames. Proceedings of the National Academy of Sciences of the United States of America 110, 11284-11289.

Ferreira, T.A., Blackman, A.V., Oyrer, J., Jayabal, S., Chung, A.J., Watt, A.J., Sjostrom, P.J., and van Meyel, D.J. (2014). Neuronal morphometry directly from bitmap images. Nat Methods 11, 982-984.

Goslin, K., and Banker, G. (1989). Experimental observations on the development of polarity by hippocampal neurons in culture. The Journal of cell biology 108, 1507-1516.

Hand, R., Bortone, D., Mattar, P., Nguyen, L., Heng, J.I., Guerrier, S., Boutt, E., Peters, E., Barnes, A.P., Parras, C., *et al.* (2005). Phosphorylation of Neurogenin2 specifies the migration properties and the dendritic morphology of pyramidal neurons in the neocortex. Neuron 48, 45-62.

Hoogenraad, C.C., Milstein, A.D., Ethell, I.M., Henkemeyer, M., and Sheng, M. (2005). GRIP1 controls dendrite morphogenesis by regulating EphB receptor trafficking. Nat Neurosci 8, 906-915.

Janssen, A.F.J., Tas, R.P., van Bergeijk, P., Oost, R., Hoogenraad, C.C., and Kapitein, L.C. (2017). Myosin-V Induces Cargo Immobilization and Clustering at the Axon Initial Segment. Front Cell Neurosci 11, 260.

Jaworski, J., Kapitein, L.C., Gouveia, S.M., Dortland, B.R., Wulf, P.S., Grigoriev, I., Camera, P., Spangler, S.A., Di Stefano, P., Demmers, J., *et al.* (2009). Dynamic microtubules regulate dendritic spine morphology and synaptic plasticity. Neuron 61, 85-100.

Kapitein, L.C., Schlager, M.A., van der Zwan, W.A., Wulf, P.S., Keijzer, N., and Hoogenraad, C.C. (2010a). Probing intracellular motor protein activity using an inducible cargo trafficking assay. Biophys J 99, 2143-2152.

Kapitein, L.C., Yau, K.W., and Hoogenraad, C.C. (2010b). Microtubule dynamics in dendritic spines. Methods Cell Biol 97, 111-132.

Kiuchi, T., Higuchi, M., Takamura, A., Maruoka, M., and Watanabe, N. (2015). Multitarget super-resolution microscopy with high-density labeling by exchangeable probes. Nat Methods 12, 743-746.

Meijering, E., Jacob, M., Sarria, J.C., Steiner, P., Hirling, H., and Unser, M. (2004). Design and validation of a tool for neurite tracing and analysis in fluorescence microscopy images. Cytometry Part A : the journal of the International Society for Analytical Cytology 58, 167-176.

Mi, H., Lazareva-Ulitsky, B., Loo, R., Kejariwal, A., Vandergriff, J., Rabkin, S., Guo, N., Muruganujan, A., Doremieux, O., Campbell, M.J., *et al.* (2005). The PANTHER database of protein families, subfamilies, functions and pathways. Nucleic Acids Res 33, D284-288.

Montojo, J., Zuberi, K., Rodriguez, H., Kazi, F., Wright, G., Donaldson, S.L., Morris, Q., and Bader, G.D. (2010). GeneMANIA Cytoscape plugin: fast gene function predictions on the desktop. Bioinformatics (Oxford, England) 26, 2927-2928.

Reimand, J., Arak, T., Adler, P., Kolberg, L., Reisberg, S., Peterson, H., and Vilo, J. (2016). g:Profiler-a web server for functional interpretation of gene lists (2016 update). Nucleic Acids Res 44, W83-89.

Schatzle, P., Kapitein, L.C., and Hoogenraad, C.C. (2016). Live imaging of microtubule dynamics in organotypic hippocampal slice cultures. Methods Cell Biol 131, 107-126.

Schindelin, J., Arganda-Carreras, I., Frise, E., Kaynig, V., Longair, M., Pietzsch, T., Preibisch, S., Rueden, C., Saalfeld, S., Schmid, B., *et al.* (2012). Fiji: an open-source platform for biological-image analysis. Nat Methods 9, 676-682.

Shannon, P., Markiel, A., Ozier, O., Baliga, N.S., Wang, J.T., Ramage, D., Amin, N., Schwikowski, B., and Ideker, T. (2003). Cytoscape: a software environment for integrated models of biomolecular interaction networks. Genome research 13, 2498-2504.

Tas, R.P., Bos, T., and Kapitein, L.C. (2018). Purification and Application of a Small Actin Probe for Single-Molecule Localization Microscopy. Methods Mol Biol 1665, 155-171.

Tortosa, E., Adolfs, Y., Fukata, M., Pasterkamp, R.J., Kapitein, L.C., and Hoogenraad, C.C. (2017). Dynamic Palmitoylation Targets MAP6 to the Axon to Promote Microtubule Stabilization during Neuronal Polarization. Neuron 94, 809-825 e807.

Yuan, B., Latek, R., Hossbach, M., Tuschl, T., and Lewitter, F. (2004). siRNA Selection Server: an automated siRNA oligonucleotide prediction server. Nucleic Acids Res 32, W130-134.